Modular Isotopic Thermoelectric Generator

A. Schock

Fairchild Space and Electronics Company
Germantown, Maryland 20767

ABSTRACT

Advanced RTG concepts utilizing improved thermoelectric materials and converter concepts are under study at Fairchild for DOE. The design described here is based on DOE's newly developed radioisotope heat source, and on an improved silicon-germanium material and a multicouple converter module under development at Syncal. Fairchild's assignment was to combine the above into an attractive power system for use in space, and to assess the specific power and other attributes of that design. The resultant design is highly modular, consisting of standard RTG slices, each producing ~24 watts at the desired output voltage of 28 volt. Thus, the design could be adapted to various space missions over a wide range of power levels, with little or no redesign. Each RTG slice consists of a 250-watt heat source module, eight multicouple thermoelectric modules, and standard sections of insulator, housing, radiator fins, and electrical circuit. The design makes it possible to check each thermoelectric module for electrical performance, thermal contact, leaktightness, and performance stability, after the generator is fully assembled; and to replace any deficient modules without disassembling the generator or perturbing the others. The RTG end sections provide the spring-loaded supports required to hold the free-standing heat source stack together during launch vibration. Detailed analysis indicates that the design offers a substantial improvement in specific power over the present generation of RTGs, using the same heat source modules.

INTRODUCTION

Over the past 20 years, Radioisotope Thermoelectric Generators (RTGs), developed under the aegis of the Department of Energy's Space and Terrestrial Systems Division (DOE/STS) or its predecessors, have been successfully used in over twenty space missions [1]. During that period, they have undergone a steady process of improvement, and this evolutionary process is continuing. Its primary goal is to increase the power-to-weight ratio of RTGs, while retaining or improving their existing safety and reliability. When promising new technological and/or design options become available, conceptual designs to take advantage of those options are prepared and analyzed. If these advanced RTG designs show sufficient likelihood of success and ultimate payoff, their development is pursued for use in future missions.

The RTGs most recently flown in space are the Multi-Hundred-Watt (MHW) units developed and built by GE [2]. These units were used to power the Voyager spacecraft, which recently sent back much new information about Jupiter, Saturn, and their moons, and which is slated to fly by Uranus before leaving the solar system. A total of 10 MHW RTGs have been flown in space, and all have exhibited excellent performance stability [3].

After the MHW units, DOE/STS pursued the development of a new, modular heat source, designated as the General-Purpose Heat Source (GPHS) because of its applicability to a wide range of energy conversion systems and power levels. The GPHS module had first been designed by Los Alamos, with analytical support from Battelle; it was later considerably modified by Fairchild [4], and is currently under development by GE with major contributions by a number of other organizations.

The latest generation of RTGs, currently under construction, is designated as the GPHS/RTG because it is built around the new General-Purpose Heat Source. It started out as a conceptual design by Fairchild [5] for DOE/STS, which was partially modified by GE [6], the DOE flight system contractor. The GPHS/RTGs are being built for use on the NASA Galileo mission, to orbit Jupiter, study its moons, and send a probe into its atmosphere; and for the NASA/ESA Solar-Polar Mission, to study the region outside the earth's ecliptic plane and above the sun's poles. First launch of the GPHS/RTG is currently scheduled for 1985.

Consideration has lately been given to more advanced and much lighter RTG designs, for use on future missions. To help this effort, DOE/STS—in the summer of 1980—asked Fairchild to prepare a new RTG design taking optimum advantage of new materials, fabrication techniques, and design concepts developed in the past few years, and to carry out an analysis to assess its potential. This work is described here.

As will be seen, the conceptual design which emerged from the Fairchild study incorporates the modular GPHS heat source mentioned earlier; a new thermoelectric material developed by Syncal (with the support of NASA/JPL and DOE/STS); a multicouple thermoelectric module concept pioneered by Syncal, demonstrated by them in a DOE/STS program, and more recently modified by Fairchild; a multi-foil thermal insulation system developed by Thermoelectron [7]; and novel concepts for the thermoelectric converter arrangement and for the heat source structural supports, developed by Fairchild.

The new thermoelectric material is obtained by the addition of 5% gallium phosphide to the previously used silicon-germanium material. The resultant SiGe/GaP material has a substantially lower thermal conductivity than SiGe, and therefore offers a significantly higher conversion efficiency.

The RTG design evolved by Fairchild is designated as the Modular Isotopic Thermoelectric Generator (MITG) for reasons explained in the next section. Fuller design details and their rationale are presented in subsequent sections. The final section lists the salient parameters of an illustrative 282-watt design, and compares its specific power with that of past and present RTGs.

OVERVIEW OF MITG DESIGN

The principal distinguishing feature of the MITG design is its modularity. The generator consists of repetitive slices of standard design, each slice producing approximately 24 watt at 28 volt (or slightly higher, if desired). Thus, the basic design is adaptable to a wide range of power levels, since the output power can be scaled in 24-watt steps by varying the number of standard generator slices, generally without any other design changes.

This scalability of the MITG is a major advance over earlier RTG designs. In the MHW generator, a change in power level would have required a major redesign and requalification of the heat source. And even with the GPHS generator, which uses the same modular heat source as the MITG, changing the power level would generally require major changes in the thermoelectric couples and circuit to maintain the same output voltage.

Each slice of the MITG generator consists of one GPHS heat source module surrounded by eight thermoelectric modules, as well as standardized sections of thermal insulation, housing, radiator fins, and electrical circuit. When varying the number of slices in the generator, the only item which may have to be redesigned is the housing. For very long generators, the cantilevered housing may require a thicker wall to withstand the bending moments caused by transverse g-loads.

After the complete converter is assembled and an electrical heater is inserted, the thermoelectric modules can be individually checked for electrical performance, for thermal contact to the generator housing, for hermeticity of their C-ring seals, and for performance stability during extended operation. If any thermoelectric modules are found to be deficient, they can be replaced without disassembling the generator or perturbing the other modules. These features are not available in past or present RTG designs. In those, it is not possible to check the performance of individual thermoelectric couples; and even if a deficient one could be identified, it could not be replaced without major disassembly of the generator.

The final distingulshing feature of the MITG design is that its electrical circuit is located outside the generator housing. The series-parallel circuit permits high redundancy against open

circuits, and—since the wiring is outside the generator—the chance of shorts-to-ground is minimized. Finally, if it were desired to produce a higher output voltage for all or part of the payload, the circuit could be arranged to do so (e.g., up to 180 V at 300 W). This option also was unavailable in previous RTG designs.

Figure 1 shows a sectioned view of the General-Purpose Heat Source (GPHS) module, which is at the center of each generator slice. The radioisotope fuel capsules are surrounded by a variety of safety provisions to ensure fuel containment under all credible accident conditions. Each heat source module has overall dimensions of roughly 3.8 x 3.7 x 2 inches, and weights 3.2 lbs. As can be seen, there are four 62.5-watt $^{238}PuO_2$ fuel pellets, giving a total thermal power of 250 W per heat source module.

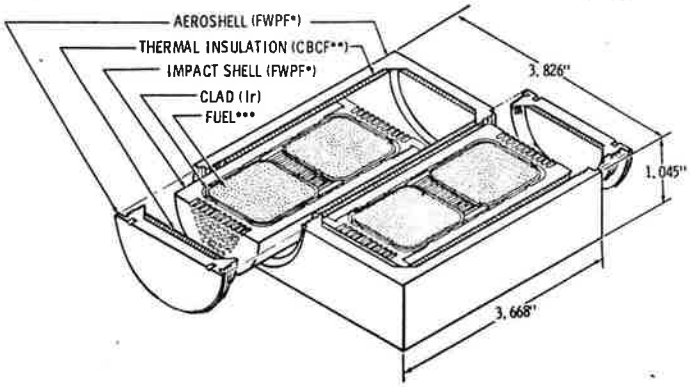

*Fine-weaved pierced fabric, a 90%-dense 3D carbon-carbon composite
**Carbon-bonded carbon fibers, a 10%-dense high-temperature insulator
***62.5-watt $^{238}PuO_2$ pellet

Figure 1. General-Purpose Heat Source Module (250 Watt) Sectioned at Mid-Plane

Each fuel pellet is contained in an iridium clad, which is expected to deform—but not breach—upon earth impact. The fuel capsules are protected by impact shells, which are designed to absorb energy by crush-up during impact; and the impact shells are protected by an aeroshell, which is designed to ablate but retain its integrity during the reentry heat pulse. There are two fuel capsules per impact shells, and two impact shells per aeroshell. Both the impact shells and the aeroshell are made of the same graphitic material, Fine-Weave Pierced Fabric (FWPF). This is a three-dimensional carbon-carbon composite of high density and strength.

Between the impact shells and the aeroshell is a layer of high-temperature thermal insulation. This consists of Carbon-Bonded Carbon Fibers (CBCF), a low-density structure with excellent insulating properties at high temperatures. The insulator is designed to prevent the fuel capsules from overheating during the reentry heat pulse and from overcooling during subsequent atmospheric descent. A much fuller explanation of the GPHS design rationale was presented in a recent paper [4].

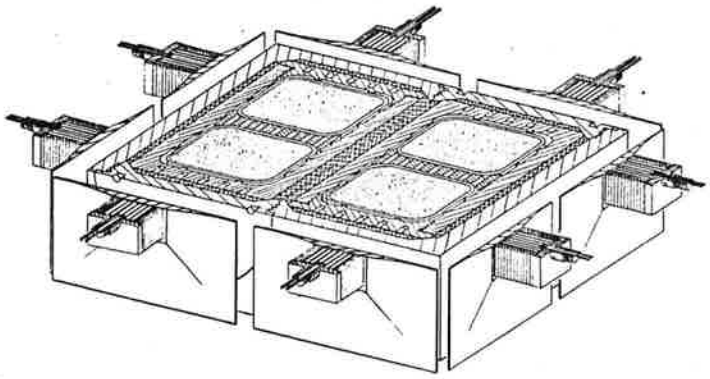

Figure 2. Heat Source Module with Its Eight Thermoelectric Modules, Sectioned at Mid-Plane

Figure 2 shows a sectioned view of the heat source surrounded by eight thermoelectric modules. The latter are described in detail in the next section. The heat source and the thermoelectric hot shoes are separated by 0.35-inch vacuum gaps, and heat transfer between them is by radiation only.

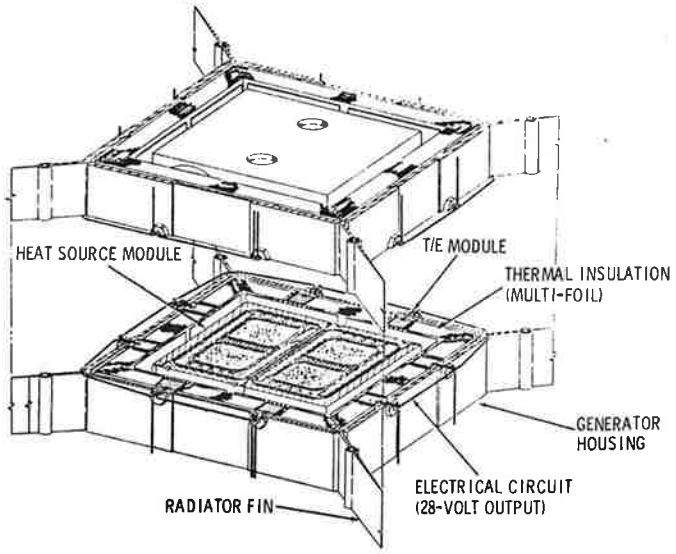

Figure 3. Typical Generator Slice (~24 Watts at 28 Volts) Split at Mid-Plane, To Display Internal Components

Figure 3 shows a complete generator slice, split at its mid-plane to display its interior components. In addition to the heat source and thermoelectric modules depicted previously, the figure shows the thermal insulation, the generator housing with attached radiator fins, and the external electrical circuit loop with its 28-volt output. Each of these subsystems is discussed in detail below.

THERMOELECTRIC MODULE DESIGN

Figure 4 shows an overview of the thermoelectric module (multi-couple), with the insulation wrap around the thermoelectric legs omitted for clarity. The module receives a heat input of approximately 30 W on its hot shoe. Most of this heat flows through the thermoelectric legs to the cold shoe. The legs have a hot-junction temperature of 1000°C (the same as in present-generation SiGe generators) and a cold-junction temperature of roughly 300°C. The terminal leads of the thermoelectric module emerge through the stud of the cold shoe, delivering an output of less than 1 amp at 3.5 volt.

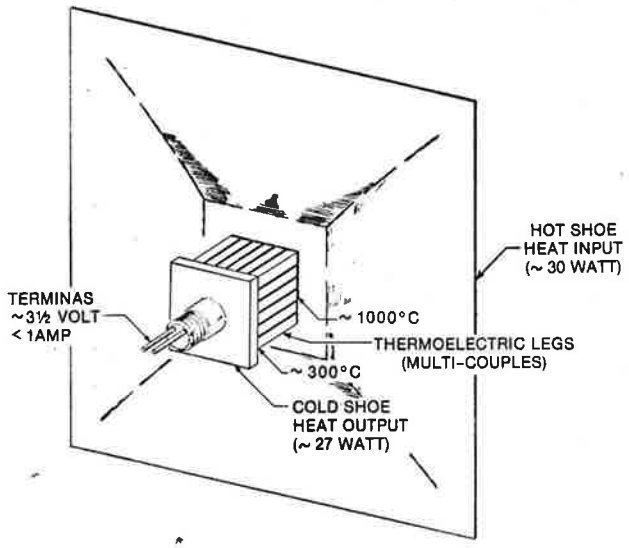

Figure 4. Thermoelectric Module (Without Insulation)

As can be seen, the thermoelectric module contains a multiplicity of legs. Assuming a desired output of 28 volt per generator slice, each of the eight series-connected thermoelectric modules must produce 3.5 volt. Based on thermoelectric property measurements at Syncal, the optimum couple voltage for SiGe/GaP operating between hot- and cold-junction temperatures of 1000° and 300°C is 0.193 volt. Thus, the 3.5-volt module output can be produced by 18 couples or 36 legs per module. As will be seen, this optimum number of legs lends itself well to a multicouple design.

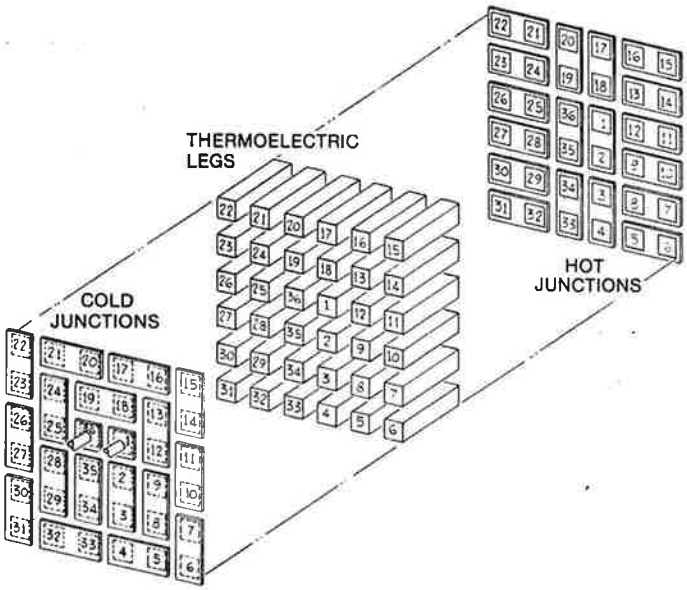

Figure 5. Thermoelectric Module Elements (Exploded View)

The arrangement of the module's 36 legs together with the required hot- and cold-junction connectors is shown in exploded view in Figure 5. The legs within a module are connected in series, as indicated by the sequential numbers. N-legs and P-legs alternate in sequence. As can be seen, the first and last legs are located at the center of the module, to facilitate the passage of the terminal leads through the cold-shoe stud, as shown earlier in Figure 4.

Figure 6 shows the components of the thermoelectric module in exploded view, with the insulator wrap again omitted. The leg assembly, whose fabrication is discussed in the next section, forms a nearly cubical block of 0.30 x 0.36 x 0.36 inches. The hot junctions consist of diffusion-bonded silicon wafers, and the cold junctions of a sputtered and photoetched tungsten coating. The 2"-square hot shoe and the cold shoe with integral stud are made of molybdenum, and the built-in terminal leads are niobium. The outer face of the cold shoe has a gold foil brazed to it, for improved thermal contact to the generator housing.

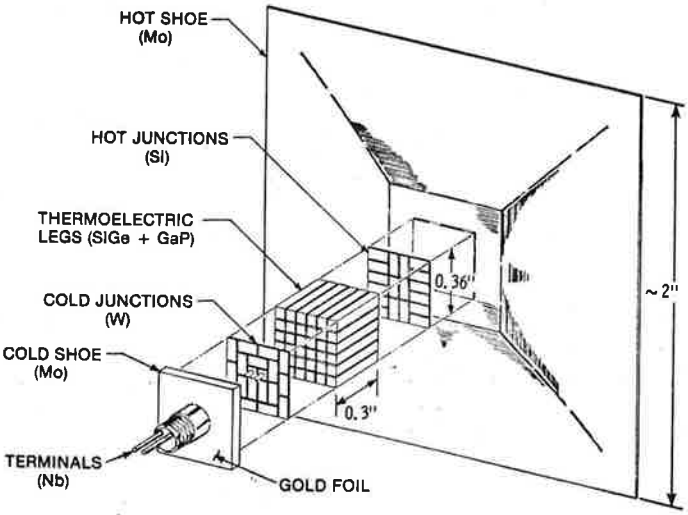

Figure 6. Thermoelectric Module Components (Insulators Not Shown)

The figures presented thus far have shown all legs as having the same cross-sectional areas. However, it can be shown that the optimum N-leg to P-leg area ratio for this material is 0.80. Figure 7 shows the effect of leg area ratio on the thermoelectric material efficiency of SiGe/GaP.

The curves show the variation of efficiency with load voltage, for the assumed hot- and cold-junction temperatures, and for 36 legs per module and 8 modules in series. The lower curve is for equal leg areas and the upper curve is for the optimum leg area ratio of 0.80. As can be seen, optimization of the leg area ratio gains approximately 0.1% in efficiency. Thus, we conclude that the use of non-uniform leg area is beneficial, but would not be essential if it proved to be too difficult to implement.

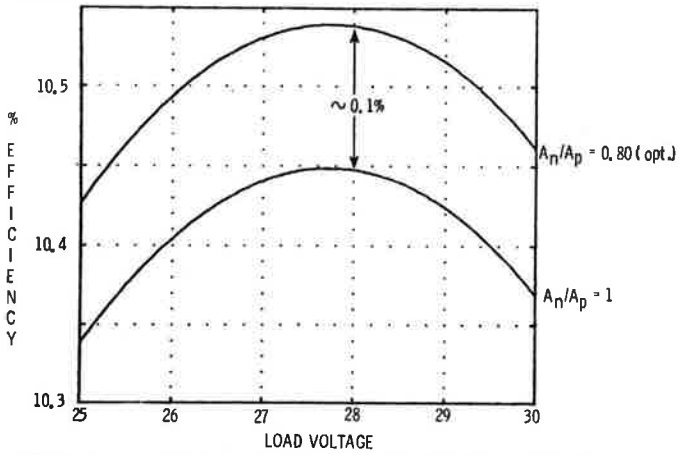

Figure 7. Effect of Area Ratio of Thermoelectric Legs On Material Efficiency of SiGe/GaP (T_H = 1000°C, T_C = 300°C, 36 Legs per Module, 8 Modules in Series)

THERMOELECTRIC MODULE FABRICATION

Figure 8 illustrates the multicouple fabrication technique developed by Syncal, and shows that this technique would indeed be applicable to the production of optimized leg areas. Starting at the top with blocks of N and P material, the first step is to cut slices of 0.051" and 0.063" thickness, respectively. These slices are individually coated with a glass layer consisting primarily of silica. Three slices of each type are assembled in an alternating array, and are fused together. The fused block is then sliced in a direction perpendicular to the bonded interfaces, to produce six slices of 0.057" thickness.

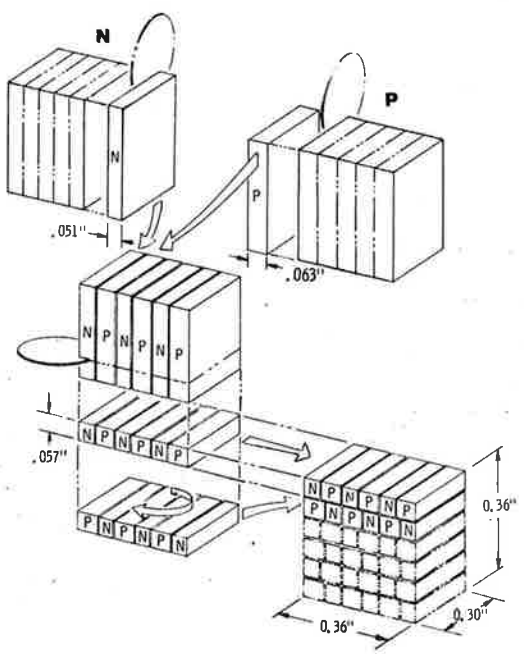

Figure 8. Fabrication of T/E Module with Optimized A_n/A_p

These slices, containing alternating N and P legs, are again coated with silica glass, and six such slices are assembled into a block in which the N and P legs form a checkerboard pattern, as shown. The slices forming this block are joined together by fusing the intervening glass layers, and the faces of the block are subsequently coated with the same glass material. Thus, the glass coating acts both as a bond and as an electrical insulator. In addition, as will be discussed later, it also serves to supress the sublimation of silicon from the hot ends of the thermoelectric legs.

The above fabrication sequence, as implemented (for equal-area legs) by Syncal Corporation, is depicted in Figure 9.

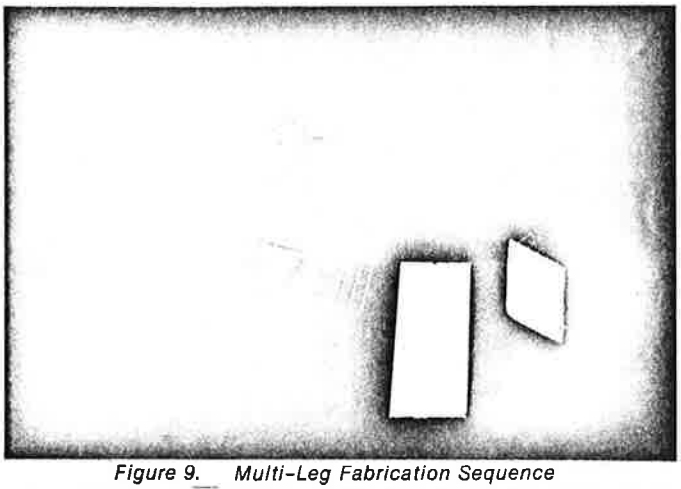

Figure 9. Multi-Leg Fabrication Sequence

As illustrated in Figure 10, the two uninsulated end faces of the block of thermoelectric legs are then covered with hot junctions and cold junctions, and the two junction faces are covered with additional glass layers, which are used to insulate them from and bond them to the hot and cold shoes of the module. A static tensile test at Syncal has demonstrated that the glass bond to the hot shoe is quite strong, in fact stronger than the thermoelectric legs themselves. But no dynamic tests to demonstrate the ability of the bond to survive launch vibration have been carried out as yet. In the author's opinion, this is the most critical unresolved feasibility issue of the MITG design at present.

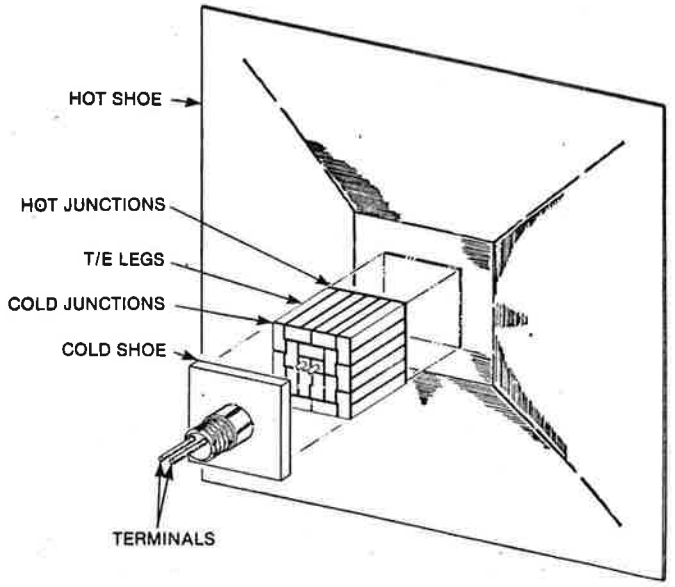

Figure 10. Thermoelectric Circuit Assembly Ready for Glass Bonding To Hot and Cold Shoes

It should be noted that all of the thermoelectric elements and all circuit elements within the generator are completely enclosed by glass coatings. In contrast to previous RTGs, the MITG hot shoes and cold shoes are electrically isolated from the thermoelectric circuit. Therefore, contact between them and the electrically grounded metallic multifoil insulation is not harmful, and the need for the previously used ceramic insulator wafers is eliminated. This saves weight, and enhances the reliability of the generator by minimizing the chance for internal shorting (e.g., by loose foil insulation particles).

In addition to its bonding and insulating function, the silica glass coating can also serve as a sublimation suppressant, since it completely covers the SiGe legs and the Si hot shoes. Silicon sublimation from the hot end of the thermoelectric legs is an important concern, because it can act as a life-limiting mechanism. In previous generators like the MHW and GPHS/RTGs, the SiGe legs were coated with silicon nitride to reduce sublimation [8]. In the present design it is expected that the glass coating will fulfill this suppression function for the required operating life.

Only limited confirmatory tests have been completed by Syncal thus far. Figure 11 shows a log-log plot of sublimation in mils vs test time in years. The test data points are indicated by open circles. Data were obtained for bare coupons at 1000°, 1050° and 1100°C, and for glass-coated coupons at 1100°C.

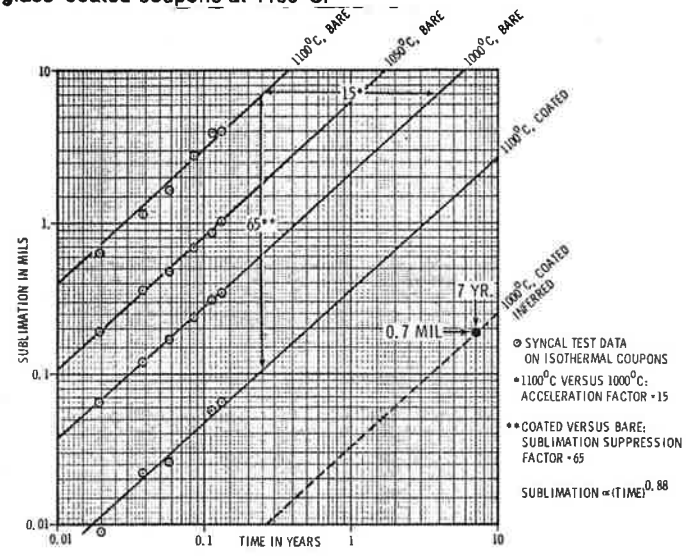

Figure 11. Effect of SiO_2 Glass Coating on SiGe-GaP Sublimation

As can be seen, all data can be fitted with straight lines having a slope of 0.88, suggesting that cumulative sublimation is proportional to the 0.88 power of time. The data for bare coupons show that sublimation is 15 times more rapid at 1100°C than at the desired hot-junction temperature of 1000°C. This acceleration factor is important, because it makes it possible to simulate the desired 7-year life in more reasonable test times. The 1100°C data indicates that the glass coating reduces the sublimation rate by a factor of 65. Assuming that the log-log curve fit can be extrapolated to long times, that the same temperature acceleration factor applies to coated samples, and that the 1100°C sublimation suppression factor also applies at 1000°C, we can infer the dashed curve for a coated sample at 1000°C. This dashed curve predicts a sublimation loss during a 7-year mission of 0.17 mils, which is only 6% of the assumed 3-mil coating thickness on the outside of the thermoelectric legs. While these results are quite encouraging, more and longer tests are clearly needed to confirm this prediction.

Figure 12 shows a photograph of a completed multicouple module, produced by Syncal by means of the above-described fabrication procedure. The experience gained there is quite encouraging. Three multicouple modules were made, with good reproducibility. Each exhibited excellent performance stability during its 3000-hour test.

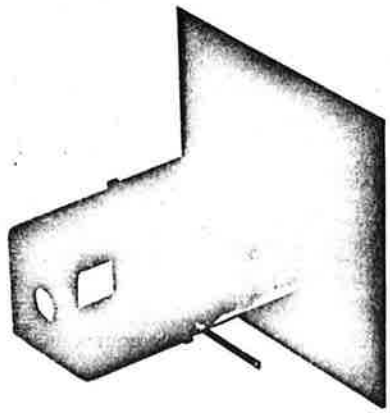

Figure 12. Multi-Couple Module Produced by Syncal

The modules produced by Syncal are generally quite similar in their arrangement and dimensions to the MITG thermoelectric module design, but differ in four respects: first, instead of the rigid cold-shoe stud called for by the MITG design, they used a compliant

cold-end heat shunt, similar to that used in the MHW generator. As will be seen, this compliant mounting arrangement is not needed in the MITG design. Second, instead of the brazed terminal leads at the center of the leg assembly postulated in the MITG design, they had their leads spot-welded to the outside of two corner legs. Such spot-welded side leads are much harder to fabricate reliably, and are more prone to failure during subsequent flexing. In the MITG design the central terminal leads are brazed in place and are rigidly supported by the cold-shoe stud. Third, the couple pictured contained 42 legs of equal area, instead of the 36 legs with optimized area ratio assumed in the MITG design. And fourth, the multicouples produced by Syncal had much smaller hot shoes (1" square) than the 2" hot shoe of the MITG design.

THERMOELECTRIC HOT SHOE

The unusually large size of the MITG hot shoe makes its design of critical importance, not only because the hot shoe is the principal weight component of the thermoelectric module, but also because the more it weighs the higher the stress on the hot-junction bonds during launch of the spacecraft. For these reasons, we wish to minimize the weight of the hot shoe by reducing its thickness. However, the thinner the hot shoe is, the higher the temperature gradients required for heat flow towards the thermoelectric legs, and the higher the temperature of the heat source surface for a given hot-junction temperature. Heat source surface temperature, however, is presently limited to 1100°C, because of concern about excessive grain growth in the iridium fuel capsule at higher heat source temperatures. The problem, therefore, is to minimize the hot-shoe weight for the specified hot-junction and heat source surface temperatures.

As illustrated in Figure 13, the use of a hot shoe of uniform thickness would be very inefficient. The figure shows the temperature map for one quadrant of a uniform-thickness hot shoe. The origin of the plot represents the center of the thermoelectric legs, and the dashed line denotes the boundary of those legs. For a 1000°C hot junction, we calculate a temperature drop of 20°C through the glass bond layer, giving a temperature of 1020°C at the center of the hot shoe. It was found that a uniform hot shoe thickness of 31 mils is required to give a heat source temperature of 1100°C. Such a hot shoe would weigh 20.5 grams, or 4.3 lb for the 96 hot shoes in a typical twelve-slice RTG. This would be a significant addition to the system weight.

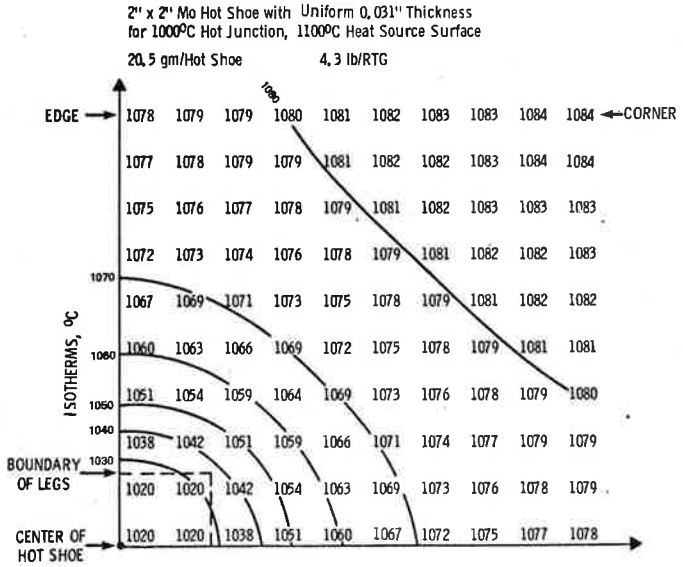

Figure 13. Temperature Distribution (°C) for Uniform Hot-Shoe

The inefficiency of a uniform thickness is shown by the isotherms, which indicate steep gradients near the center of the hot shoe and very little temperature variation near the outside. Clearly, it would be beneficial to remove material from the outer regions and add it to the inner. Such a graded-thickness design is illustrated in Figure 14, which is the result of an iterative optimization.

The dashed line shows the optimum-thickness profile, and the solid steps represent the analytical model used for the thermal analysis. This thickness profile yields a heat source surface temperature of 1100°C, and the resultant temperature map for the hot-shoe quadrant is depicted in Figure 15. Note that for this

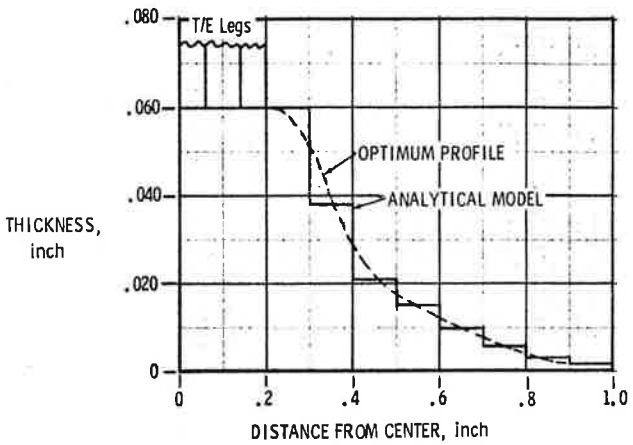

Figure 14. Optimum Hot-Shoe Profile for 1000°C Hot Junction and 1100°C Heat Source Surface

optimized design, the corner of the hot shoe is only 4°C below the temperature of the heat source surface.

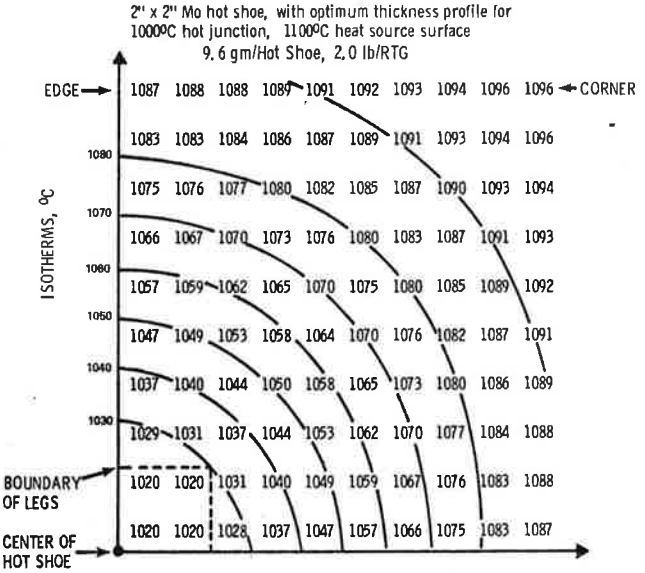

Figure 15. Temperature Distribution (°C) for Tapered Hot-Shoe

Comparison of the isotherms in Figures 13 and 15 shows that the tapered design is much more efficient, producing uniform temperature gradients everywhere except near the corner of the hot shoe. Indeed, this design weighs only 9.6 grams per hot shoe or 2.0 lbs per RTG, which is 53% lighter than the uniform-thickness hot shoe.

A cross-sectional view of the thermoelectric module with the optimum hot shoe profile is displayed in Figure 16. The figure also shows three layers of 0.012" quartz yarn surrounding the thermoelectric-leg assembly. This yarn wrap had been omitted in previous figures.

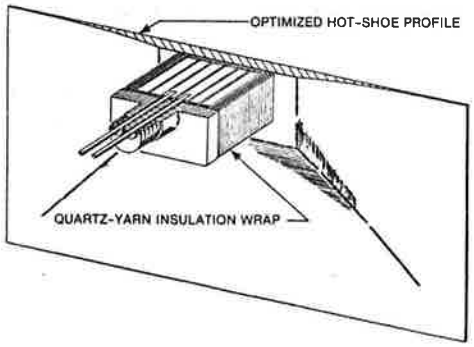

Figure 16. Cross-Sectioned Thermoelectric Module

An optional additional feature, not shown in previous or subsequent figures, is illustrated by the close-up view of the thermoelectric module shown in Figure 17. This is the addition of very thin diagnostic thermocouples for *in-situ* measurement of the module's hot-shoe and cold-shoe temperatures. The hot-shoe thermocouple leads are covered by the quartz yarn insulation wrap, and the sheathed leads for both thermocouples emerge through the cold-shoe stud. This avoids the need for additional penetrations through the thermal insulation or through the generator housing, and minimizes the danger of internal shorts.

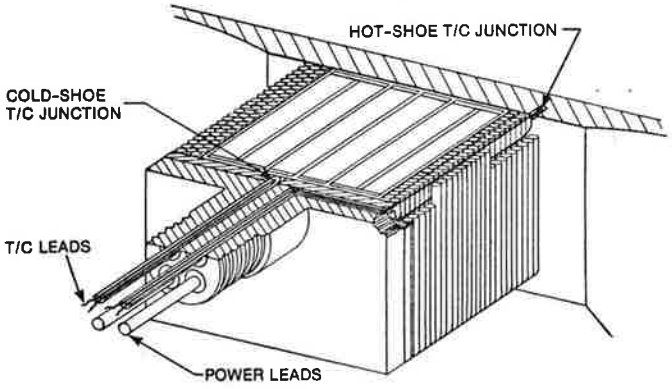

Figure 17. Built-In Thermocouples To Monitor Hot- and Cold-Shoe Temperatures

The ability to instrument each multicouple would be a very desirable feature for development testing, and would also be quite useful for flight hardware. It would make it possible to monitor the hot- and cold-junction temperatures of each thermoelectric module in the assembled generator, and would quickly identify any deficient bonds or excessive contact resistance between the cold shoe and the generator housing.

MITG HOUSING AND RADIATOR FINS

The thermoelectric modules described in the preceding section are mounted on the inside of the thermally-insulated generator wall. The thermal insulation system is discussed in the next section, and the techniques for installing the insulation and the thermoelectric modules in the housing are described in the following section.

The MITG housing has a square cross-section, to match the almost-square heat source stack. To achieve the desired cold-junction temperature, fins must be added to provide additional radiator area. The current-generation GPHS/RTGs have eight fins, which results in considerable mutual blockage and a relatively high radiator weight. The MITG design uses only four fins, giving each a relatively unobstructed view to space.

The four radiator fins could be located either as axial ribs, along the mid-line of the generator housing sides, or as diagonal fins, connected to the corners of the generator housing. These two options are compared in Figure 18, which shows the effect of fin length on the average view factor to space of the housing and of the fins.

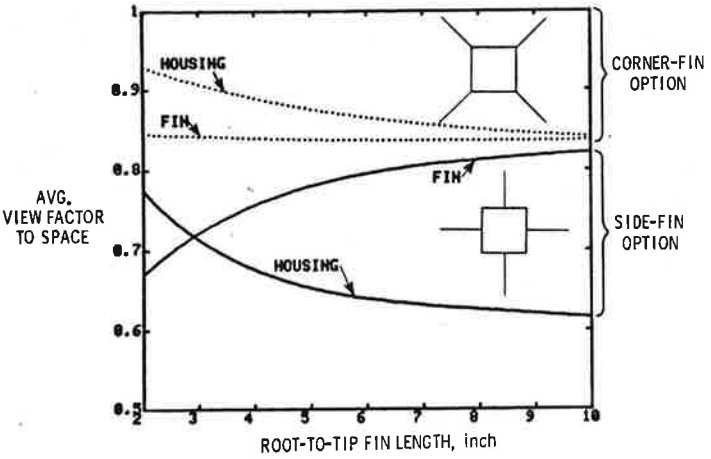

Figure 18. Location of Radiator Fins on RTG Housing

. The view factors shown are all considerably higher than what would be possible with eight fins. As can be seen, the corner fins are much more effective than the side fins, particularly because the housing has a much better view of space with the corner-fin arrangement. The housing, of course, is itself an important part of the radiator.

The superiority of the corner-fin arrangement is confirmed in Figure 19, which shows the required fin dimensions for the two options (for the desired 300°C cold-junction temperature). The fins are assumed to be trapezoidal, with a minimum fin tip thickness of 15 mils, and with the fin root thickness and fin length optimized to minimize their weight. As shown, the corner fins are shorter, thinner, and weigh 37% less than the side fins.

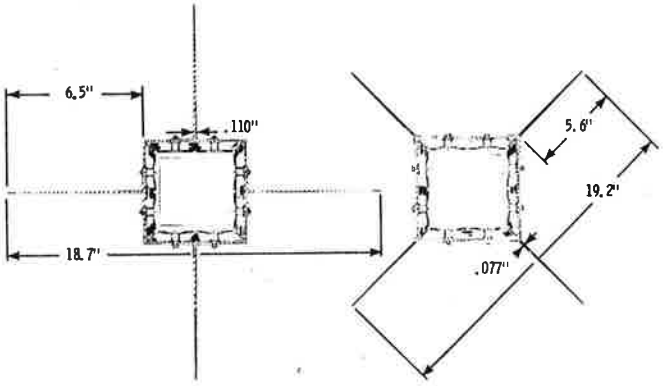

Figure 19. Comparison of Side and Corner Fins (Dimensions Shown Are Optimized for 300°C Cold-Junction Temperature and 0.015" Fin Tip Thickness)

Figure 20 shows a section of the generator housing with truncated corner fins. The figure shows an auxiliary coolant duct near the base on each fin. These ducts carry water for cooling the generator housing while the spacecraft is inside the shuttle, but are not needed during operation in open space.

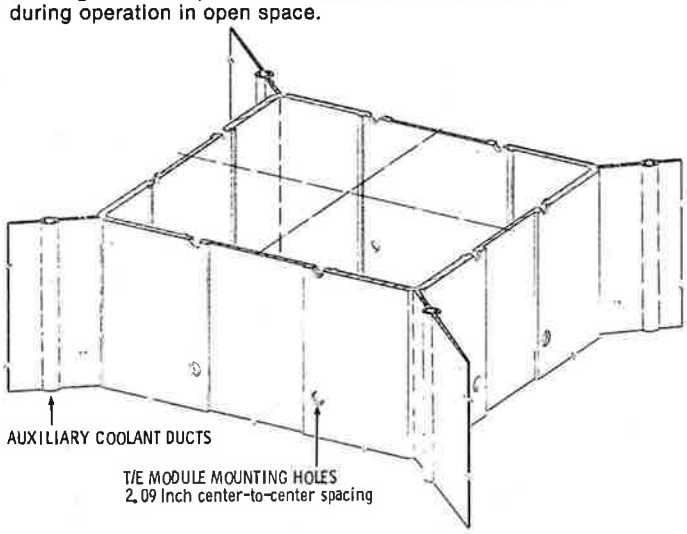

Figure 20. Generator Housing Section with Corner Fins

The housing sides have holes for mounting the thermoelectric modules, with a 2.09" center-to-center spacing between holes. Each side wall has a thickness of 1/16" near its center, and 1/8" near the corners, to accomodate heat flow from the thermoelectric modules to the radiator fins without excessive temperature drops. These thickened edge regions are fortuitous, because they strengthen and stiffen the generator housing, which plays the structural role of a cantilevered box beam.

THERMAL INSULATION

RTGs require thermal insulation to minimize the heat flow from the thermoelectric hot shoe to the generator housing. The thermal insulation used in the MITG consists of many layers of very thin metal foils, separated by spacers. This type of insulation has been used extensively, and has proven highly effective in reducing

radiative heat transfer in a vacuum environment. Multifoil insulation had also been used in the MHW and GPHS/RTGs. These generators used 60 layers of 0.3 mil molybdenum, with alternating layers of open-weave quartz cloth.

In the MITG design the quartz cloth spacers have been replaced by a low-density coating of zirconia particles. This reduces the thickness of the 60-foil package from 0.7 to 0.3 inch, and decreases the insulation weight by more than 50%. The weight reduction is itself important, because the insulation package is an important component of the generator weight; and the thickness reduction results in additional weight saving, by shrinking the size of the required generator housing and allowing the use of shorter thermoelectric legs. Multifoil insulation with zirconia particle spacers has been in use by Thermoelectron for a number of years, and has shown excellent performance stability [9]. Some multifoil assemblies of this type have also been vibration-tested, to confirm that the spacer particles will stay in place during launch vibration.

The multifoil insulation in the generator is supported by the thermoelectric modules, which in turn are mounted on the generator housing. The support provided by the thermoelectric legs is quite rigid, though there is some compliance provided by the three layers of quartz yarn wrap. While the SiGe legs are relatively strong, excessive shear loads must be avoided. The effect of differences in thermal expansion between the hot and cold foils and the aluminum housing must therefore be examined.

Figure 23 shows a typical temperature distribution for the 60 foils between 1000°C and 300°C. While previous RTGs have used molybdenum foils, the use of other materials is under consideration for the MITG. The figure illustrates a possible combination showing the use of nioblum for the hottest 32 layers, followed by 25 layers of titanium or vanadium, with the three coolest layers consisting of aluminum. The advantage of these materials is not only the potential weight reduction of the foil package, but also their better thermal expansion match to the aluminum housing.

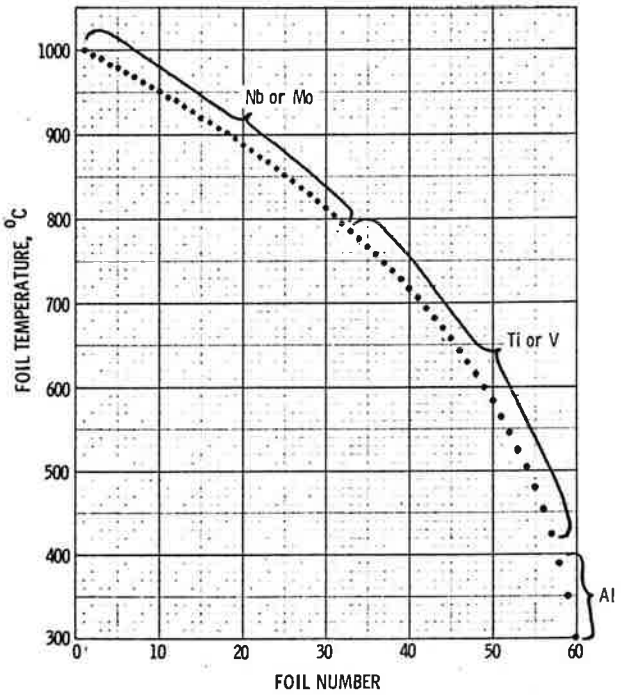

Figure 21. Multifoil Insulation Temperature Distribution

Figure 22 shows the thermal expansion of the different foils relative to the housing. The circled points denote the material choices suggested in Figure 21. Relative expansions are given in mils per inch, but since the thermoelectric modules have a center to center spacing of 2", and the midpoint between two modules may be considered as a neutral point, the vertical scale also represents the expansion mismatch in mils at the interface between the foils and the thermoelectric module wrap.

As can be seen, the mismatch for the proposed materials is less than three mils, which can be accommodated by the compliance of the foils and the quartz yarn wrap. Thus, it is feasible to use small patches of foil with 2 x 2 thermoelectric module penetrations. But for larger foil areas, expansion joints will probably be needed to avoid excessive shear loads on the thermoelectric modules. The design of

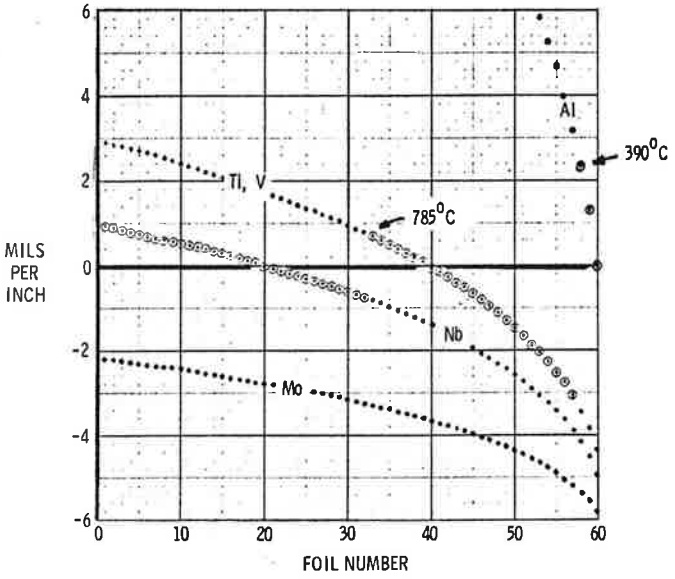

Figure 22. Thermal Expansion of Foils Relative To Housing

these expansion joints is critical, because heat loss through poorly designed joints can be much larger than losses through the unbroken areas of the foil package.

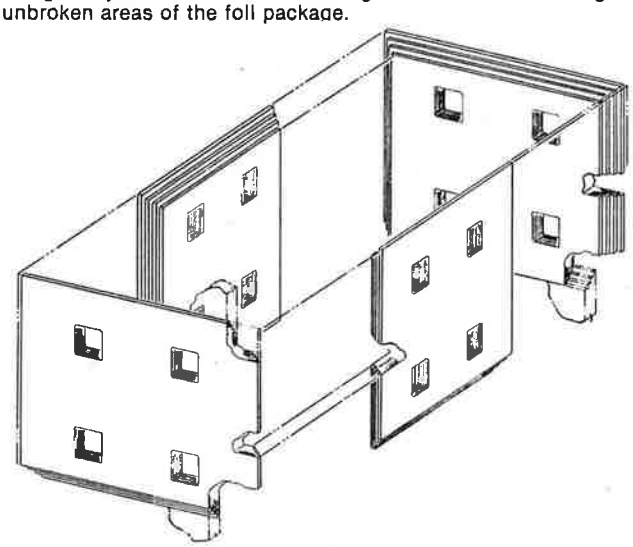

Figure 23. Multifoil Arrangement with Stepped Joints

Figure 23 shows one possible foil arrangement, using stepped joints between 4-hole multifoil sections. This arrangement, which has been used in the past, would be relatively simple to apply, but not as effective thermally as some of the other options considered.

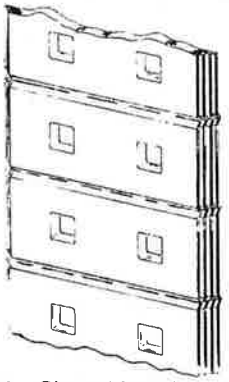

Figure 24. Pleated Multifoil Arrangement

Figure 24 illustrates a pleated foil arrangement. With this arrangement, the entire foil package for each side of the generator could be assembled as a unit, with step joints used at the edges of

the generator. The pleats would provide enough axial compliance to compensate for differential thermal expansion in that direction, and would also provide lateral stiffening to resist g-loads normal to the plane of the foil package. When the pleated foil package of this type is inserted into the snug-fitting generator housing, a rather stable structure would result, as depicted in Figure 25.

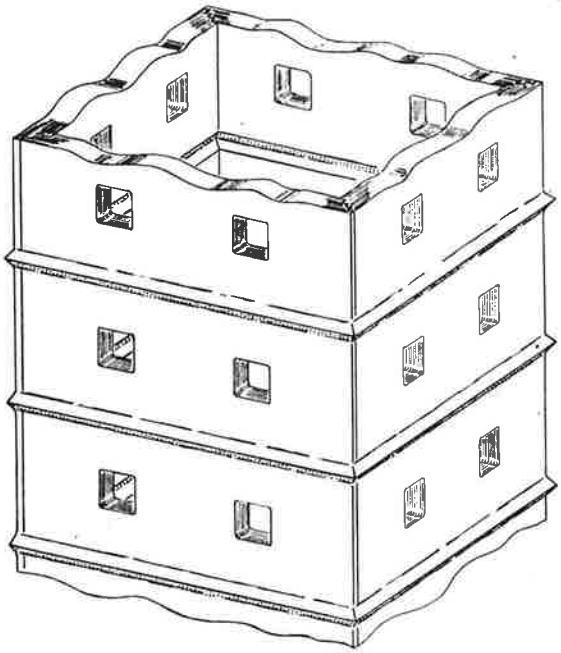

Figure 25. Multifoil Insulation Assembly Showing Axial Compliance and Lateral Stiffness Provided by Pleats

A third option, illustrated in Figure 26, would result in the lowest possible heat losses at the joints. This option, which was suggested by Thermoelectron, makes use of interleaved foils at all edges and at other expansion joints. The foil is applied in patches, each containing 2 x 2 thermoelectric module penetrations. As shown by the two cut-away sections, each foil patch is oversized to provide overlaps with neighboring foils axially, and is provided with edge flaps to provide overlaps with foils around the corner. For this design, the foil packages must be laid up one patch at a time to provide the desired interleaving. While this assembly procedure is time-consuming, it is quite feasible and is currently the preferred approach because it minimizes parasitic heat losses.

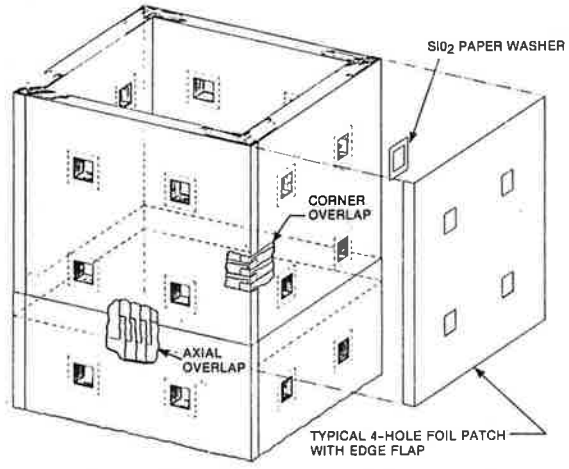

Figure 26. Interleaved Multifoil Assembly

The figure also shows a dashed square around each of the foil windows. These squares represent the outer edges of molybdenum-opacified SiO_2 paper washers, which alternate with the metal foils. Such washers have been successfully used by General Atomics in RTG development tests. In the MITG design, they help to maintain the desired 5-mil spacing between the 0.3-mil molybdenum foils, particularly during the insertion of the thermoelectric modules.

It may also be desirable to make the windows slightly over-sized in the metal foils, but not in the SiO_2 paper washers. This would allow some movement by the metal foils to accommodate differential thermal expansion, while the snug-fitting paper washers prevent interface gaps through which radiation streaming could occur.

CONVERTER ASSEMBLY PROCEDURE

This section describes the assembly and installation of the interleaved multifoil insulation in the housing of a typical 12-slice MITG, and the subsequent installation of the thermoelectric modules. These installation procedures are illustrated by the sequential Steps 1 through 8 shown in the cross-sectional plan view shown in Figure 27.

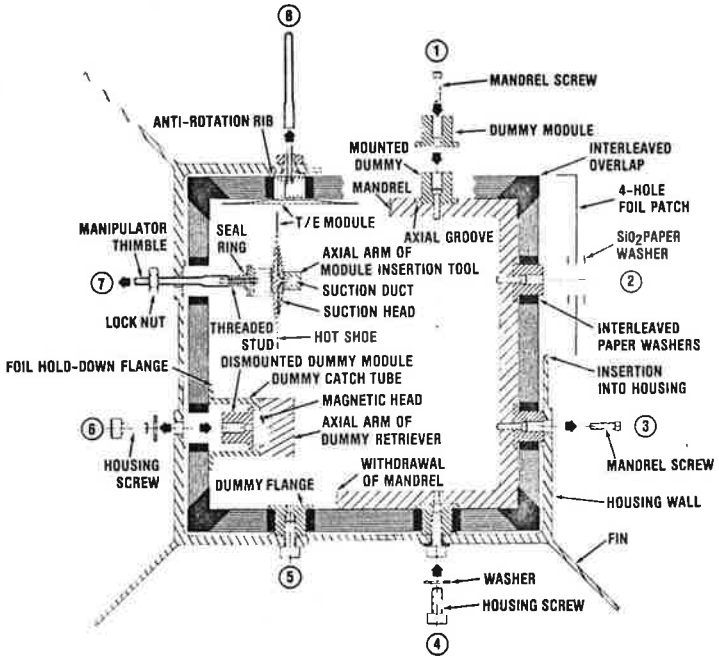

Figure 27. Converter Assembly Procedure

Step 1 shows a dummy module, with a square stud matching the dimensions of the yarn-wrapped leg assembly and the cold shoe of the thermoelectric module. Also depicted is a small screw for attaching the dummy module to the central mandrel, as shown.

The mandrel has a square cross-section, and its outer dimensions match the desired inside dimensions of the multifoil insulation package. It extends over the full height of the generator, and contains 96 threaded holes at the desired thermoelectric module locations. As shown, the mandrel has eight shallow axial grooves, which accommodate the thin flanges at the inner ends of the dummy modules.

After all 96 dummy modules have been mounted on the mandrel, it is inserted into the generator housing to make certain that there is no hang-up during insertion, and that the dummy module centers are in proper registry with the housing wall holes. The mandrel is then withdrawn, for application of the multifoil insulation.

The exploded portion of Step 2 shows two of the square SiO_2 paper washers (see Fig. 26) and a section of a 4-hole foil patch with its bent edge flap, ready for mounting on the dummy-covered mandrel. These foil patches are prepared by clamping a large number of foil layers between two rigid plates with four square windows, and broaching or milling the required foil penetrations. Each individual foil patch is then bent to form the flap for the desired edge overlap.

The foil patches are deposited on the mandrel, with the four holes of each patch slipped over the square studs of four dummy modules. They are applied individually, one complete circumferential and axial layer at a time, to give the interleaving at the axial and edge overlaps, as illustrated in Figure 26. Deposition of the foil layers alternates with installation of the SiO_2 paper washers. The assembled view shown in Step 2 of Figure 27 represents the mandrel, covered with a complete 60-layer foil assembly, ready for insertion into the MITG housing.

In Step 3, the foil-covered mandrel is inside the generator housing. The housing wall has 96 threaded holes, which line up with the small screws that attach the dummy modules to the mandrel. The housing wall holes are large enough to permit removal of the small mandrel screws from the outside of the MITG housing, as illustrated.

The small-diameter mandrel screw removed in Step 3 is replaced in Step 4 by a larger-diameter screw and washer, which fastens the dummy module to the inside of the housing wall. This screw replacement is completed for one dummy at a time, to make certain that proper registry between the multifoil penetrations and the housing wall holes is maintained.

After all 96 dummy modules have been fastened to the inside of the housing wall, the inner mandrel is free to be axially withdrawn from the insulated housing. During this withdrawal, the dummy modules serve as lateral guides for the grooved mandrel. As shown in Step 5, this leaves the multifoil package anchored to the housing wall, in proper alignment. The flanges of the dummy modules keep the foils from slipping off their inner ends.

Step 6 illustrates the removal of one of the dummy modules. After the housing screw is removed, the unfastened dummy is pushed inward by inserting a thin tool through the housing wall hole. At the same time, a flanged tube-like tool is used to keep the foils from also moving inward, and to catch the detached dummy module for axial removal. As shown, this step leaves an empty multifoil window, in registry with the corresponding housing wall hole.

Step 7 illustrates the installation of a real thermoelectric module, pictured earlier in Figure 16; through the empty multifoil window. Note that a small metal C-ring has been placed around the module's cold-shoe stud, and that a manipulator thimble has been attached to the end of that stud. This thimble serves to protect the power leads and thermocouple leads during the module insertion step, and makes possible the manual positioning of the T/E module while its cold shoe and legs pass through the foil package.

As shown in Step 7, the thermoelectric module is initially held at the center of its hot shoe, by a vacuum suction head attached to the axial arm of the module insertion tool. This tool first lines the module up with the housing hole. The alignment can be visually checked from the outside, through the hole. The tool then moves the T/E module outward, until the end of the thimble emerges from the hole. The module is then picked up manually by means of the attached thimble, and is uncoupled from the insertion tool.

Final insertion of the T/E cold shoe and yarn-wrapped leg assembly into the multifoil hole is carried out manually. This provides tactile feedback to tell the operator whether the operation is proceeding smoothly, and allows him to make final adjustments in module position, if necessary.

After the module has been fully inserted, it is locked in place by the external nut, while the T/E module is kept from rotating by the anti-rotation rib on the inside of the generator housing. This is illustrated in Step 8 of Figure 27, which also shows the subsequent removal of the manipulator thimble.

The replacement of each dummy module by a real module, as illustrated in Steps 6 through 8, must of course be completed one module at a time, to ensure retention of proper multifoil alignment.

A more detailed depiction of the mounting of the thermoelectric module to the insulated wall of the generator housing is presented in exploded view in Figure 28 and in assembled view in Figure 29.

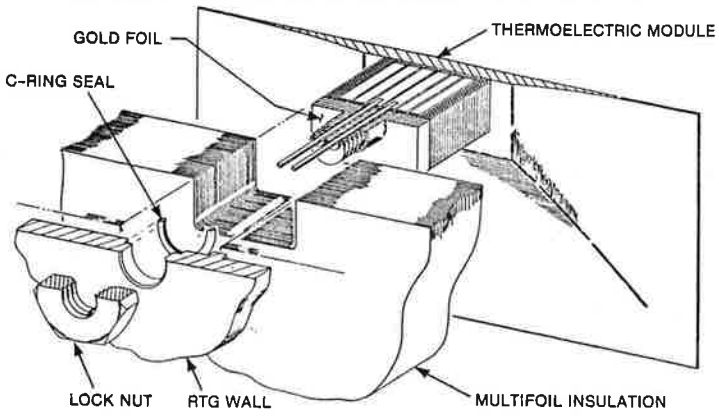

Figure 28. Mounting and Sealing Arrangement (Exploded View)

These figures show more clearly how the thermoelectric modules are locked in their mounted position by an external nut which engages the threaded cold-shoe stud, and how the housing penetration is sealed by means of a small C-ring. As in previous RTGs, the Inconel C-rings are plated with gold and silver coatings, to promote sealing. The seals must be good enough to prevent excessive losses of the inert cover gas during pre-launch and launch operations. This cover gas prevents the infusion of air while the generator is in the earth's atmosphere. The seals are not needed in space.

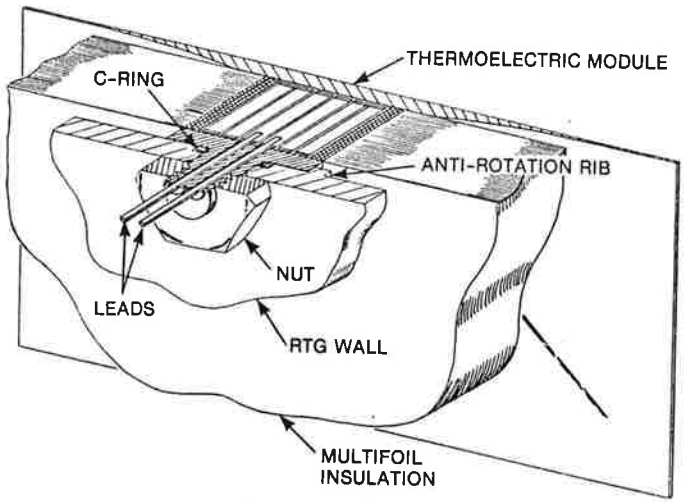

Figure 29. Mounted Thermoelectric Module

Thermal contact between the thermoelectric cold shoe and the housing wall is promoted by the compliant gold foil, and by the differential thermal expansion which greatly increases the contact pressure when the aluminum housing heats up after fueling.

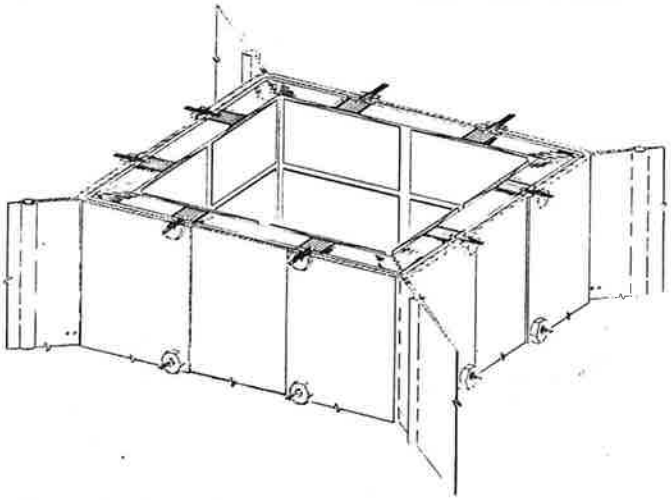

Figure 30. Assembled Converted, Showing Central Heater Cavity Formed by Hot Shoes

Figure 30 shows a sectioned view of the assembled converter, with all modules mounted on the insulated housing. The thermoelectric hot shoes form a central cavity, ready to receive an electrical heater. By means of such a heater, the full-length converter is outgassed, brought up to operating temperature, and each thermoelectric module individually checked for its electrical performance and performance stability. Each module can also be checked for leaktightness of its C-ring seal, and for thermal conductance between its cold shoe and the housing wall. Thus, any deficient module can be identified and subsequently replaced without perturbing any of the others, by reversing Steps 7 and 8 of Figure 27.

ELECTRICAL CIRCUIT

Figure 31 shows a typical converter slice with the external electrical circuit added. The figure illustrates the most basic circuit arrangement. The eight thermoelectric modules are connected in series by the loop circling the generator slice. Relatively small wires and crimped connectors can be used, since the loop carries less than 1 amp. Two of the vertical wires represent the 28-volt busbars, which connect all the generator slices in parallel. The additional vertical wires normally carry no current. They are present to form a series-parallel network, which makes the circuit highly resistant to open-circuit failures.

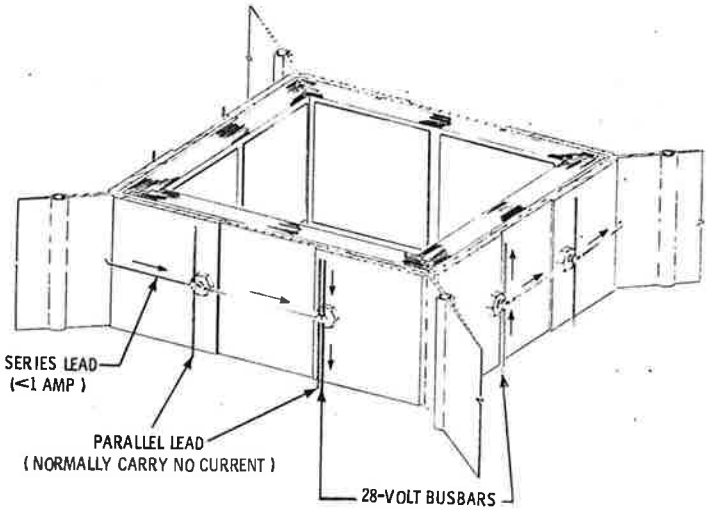

Figure 31. Standard Converter Slice with Basic Circuit Module

A slightly more complicated circuit option is illustrated in Fig. 32. For many NASA missions it is important to minimize the generator-induced magnetic field, to avoid interference with scientific instrumentation on the spacecraft. The figure illustrates a design in which the self-induced field is essentially completely eliminated. At the end of the current loop which connects the eight T/E modules in series, the current is brought back through a reverse loop, so that the two busbars are located adjacent to each other. This essentially cancels the induced magnetic field.

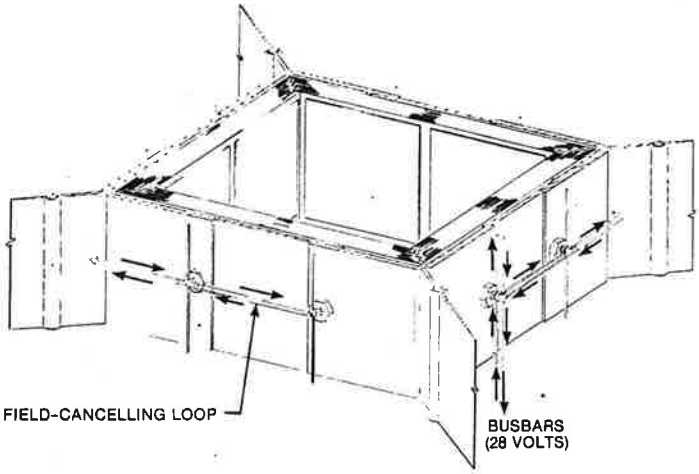

Figure 32. Standard Converter Slice with Field-Cancelling Circuit Module

Since the electrical circuit in the MITG is located outside the generator housing, there is some concern about the effect of micrometeorite impacts on circuit integrity. This problem was studied using the analytical model for meteorite impacts for NASA's Solar-Polar Mission. That model is displayed in Figure 33, which shows a plot of meteorite fluence versus particle mass.

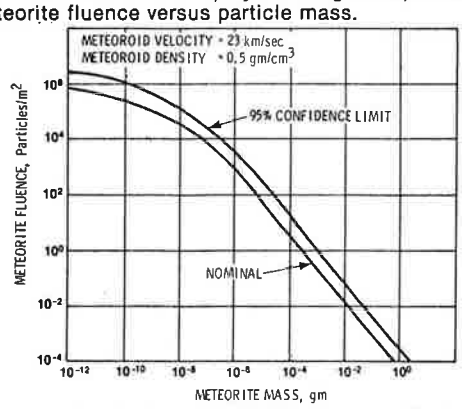

Figure 33. ISPM Meteorite Environment Model

The study showed that the reliability of the circuit against micrometeorite effects can be greatly enhanced by simple additions to the basic circuit shown earlier in Figure 31. Figure 34 shows a schematic diagram of the complete circuit for a 12-slice generator, with the 96 thermoelectric modules arranged in a 8 x 12 series-parallel array. The basic circuit elements are shown by solid lines, and the circuit additions for enhanced reliability against meteorites are shown by dashed lines. These additions consist of two items: parallelization of the busbars, with cross connectors between the two parallel busbar leads at each of the 12 slices; and the addition of parallel connectors at the second terminal of each of the thermoelectric modules.

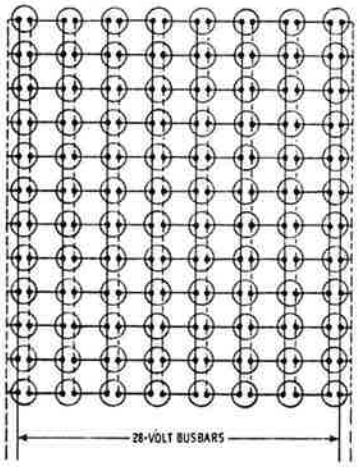

Figure 34. Redundant Circuit Additions (_ _ _ _) for Enhanced Reliability Against Meteorites

The benefit of the redundant busbars is obvious, since—without them—micrometeorite impacts could cut the single busbar and cause a major fraction of thermoelectric modules to be lost from the circuit. As we will see, this is far less likely with redundant busbars.

The addition of the other redundant connectors (shown by dashed lines) is less important, but also beneficial. Without those redundant parallel cross-connectors, the loss of any series-connector would terminate the contribution of the thermoelectric module to the left of that connector. With the addition of the redundant parallel connectors, loss of a thermoelectric module would only occur if all three wires to one of its terminals were broken, an extremely unlikely event.

The analytical predictions for meteorite impact effects on both the basic circuit and the redundant (improved) design are summarized in Table 1. For each option, the table lists the results for the busbars and for the remainder of the network. The table lists the wire gauge and diameter of the stranded connectors, as well as the resultant circuit weight and ohmic loss.

Table 1. Influence of Circuit Design on Meteorite Impact Effects

Based On Meteorite Model For Solar-Polar Mission	BASIC DESIGN		REDUNDANT DESIGN	
	BUSBARS	NETWORK	BUSBARS	NETWORK
Parallel Wires	1	12	2	12
Wire Gauge (stranded)	#9	#21	#12	#21
Wire Diameter (equivalent)	0.114 in	0.028 in	0.081 in	0.028 in
Wire Length (total)	4 ft	39 ft	8 ft	55 ft
Wire Weight	0.16 lb	0.19 lb	0.16 lb	0.27 lb
Ohmic Loss	0.087% 0.24w	0.092% 0.26w	0.087% 0.24w	0.092% 0.26w
Total-Failure Probability*	0.00072	Negligible	0.00000013	Negligible
Survival Probability*	0.9993	~1	0.9999999	~1
Probability of Losing One or More T/E Modules*	-	0.106	-	0.000039
Non-Degradation*-Probability	-	0.89	-	0.99996

*due to micrometeoroid impacts on circuit

As can be seen, the circuit weight is very low for all cases, because of the low current handled. Similarly, the ohmic loss is less than 0.2% of the generated power, for either option. The analytical results show that the probability of not encountering a break in any of the busbars is quite high (three 9's) even for the basic circuit design, and is extremely high (seven 9's) for the redundant design. The

probability of total failure due to damage of the rest of the network is negligible for both designs. Finally, the probability of losing the power output of one or more of the generator's 96 thermoelectric modules (due to micrometeorite impact) is 11% for the basic circuit design, and only 0.004% for the redundant design.

Clearly, the redundant design is worth using, since it adds minimal weight and no ohmic losses to the system, and yields a very high reliability. A typical converter slice with the redundant circuit is depicted in Figure 35. It shows the duplicate busbars and the added parallel connectors.

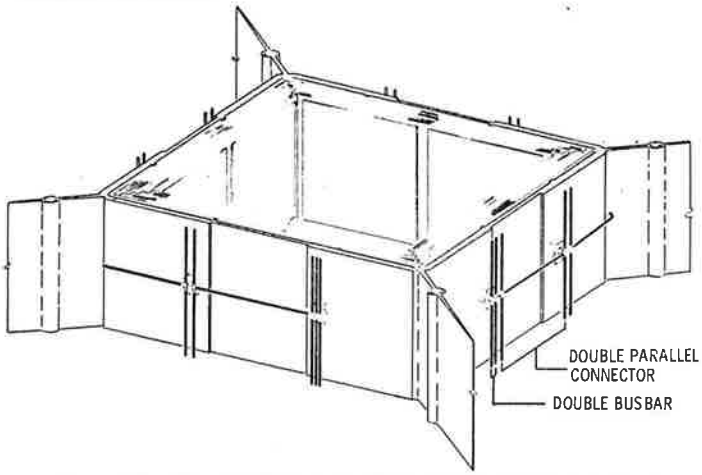

Figure 35. Standard Converter Slice with Redundant Circuit

One other circuit option should be mentioned. Historically, RTGs have been designed for an output of 28 to 30 volt, because much of the available payload equipment falls into that range. However, there are many applications, particularly at higher power levels, in which only the housekeeping equipment operates at that voltage, while the major power consumers of the payload would prefer a much higher voltage from the generator. With the multicouple design, the circuit could readily be modified to provide much higher output voltages; e.g., up to 180 V at 300 W. Alternatively, the circuit could be arranged to deliver part of the power at 28 volts for housekeeping, and part at a higher voltage for the other payload.

HEAT SOURCE SUPPORT

After the electrical circuit has been installed on the outside of the generator housing, the converter is ready for fueling, using the heat source modules pictured earlier in Figure 1. Figure 36 shows a typical slice of the MITG generator, producing approximately 24 watt at 28 volt. An MITG design for a given power output is obtained by combining an appropriate number of such standard slices, and adding the necessary end sections to complete the generator.

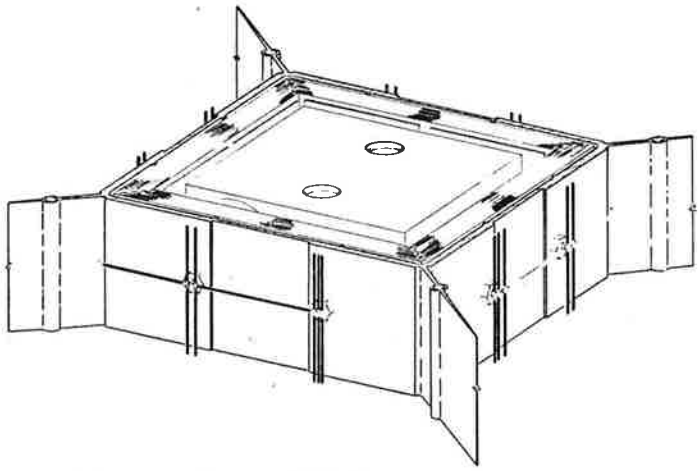

Figure 36. Standard MITG Slice (~24 Watts at 28 Volt)

Figure 37 shows a view of the generator housing, including its end flanges, the mounting bushings at the base of the fins, and the auxiliary coolant loop. This coolant loop is not needed in space, but serves to maintain the generator housing within prescribed temperature limits while it is within the shuttle bay.

Figure 38 depicts a full-length generator housing, together with a

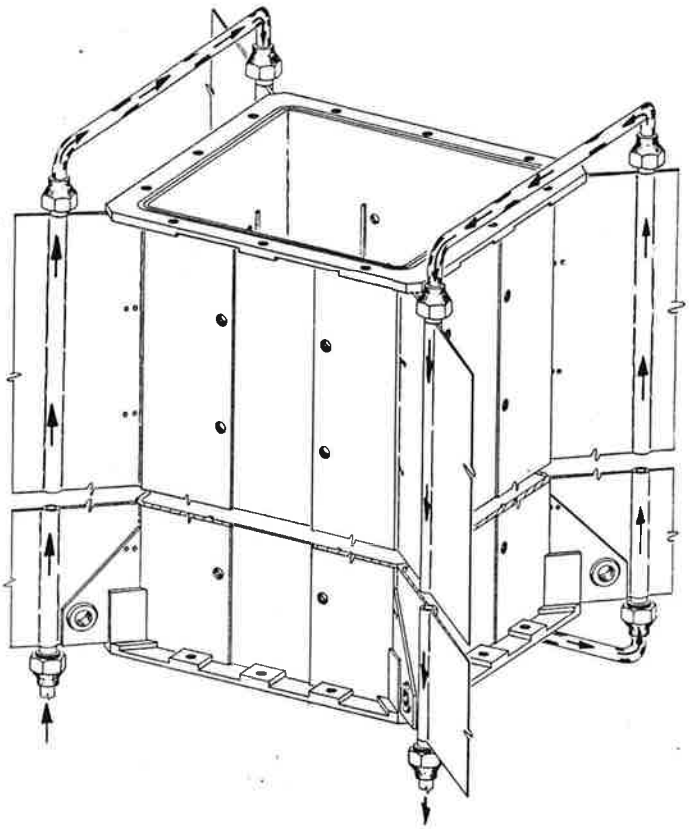

Figure 37. MITG Housing, with Auxiliary Coolant Ducts

typical heat source consisting of 12 GPHS modules. Structural support of this heat source stack is a critical problem, since it is only supported at its ends and there are no intermediate lateral supports. Very high axial preloads, on the order of 3000 lbs, are required to keep the modules from coming apart under the influence of transverse g-loads experienced during launch (typically 40 grms). This problem was discussed in great detail in earlier Fairchild papers [10, 11] and only the MITG design solution will be presented here.

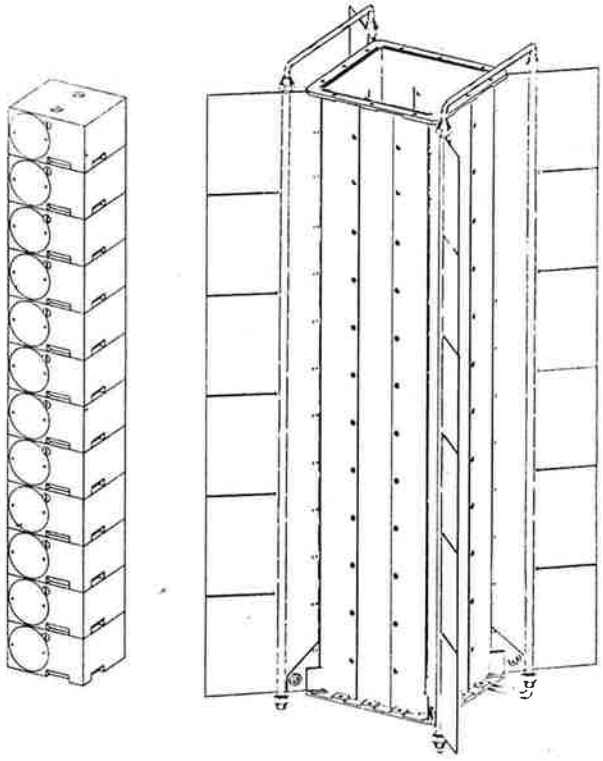

Figure 38. Heat Source Stack and Generator Housing

The basic heat source support hardware is depicted in Figure 39. The two heat source modules shown represent, of course, a much longer stack. At each corner of the heat source stack is a refractory-metal load spreader, which is contacted by a pyrolytic graphite button. Pyrolytic graphite is an excellent support material, because of its very low thermal conductivity in the C-direction (normal to the deposition plane) and because of its high strength at high temperatures. By orienting these buttons in a space-diagonal direction as shown, the required number of buttons is reduced to a minimum.

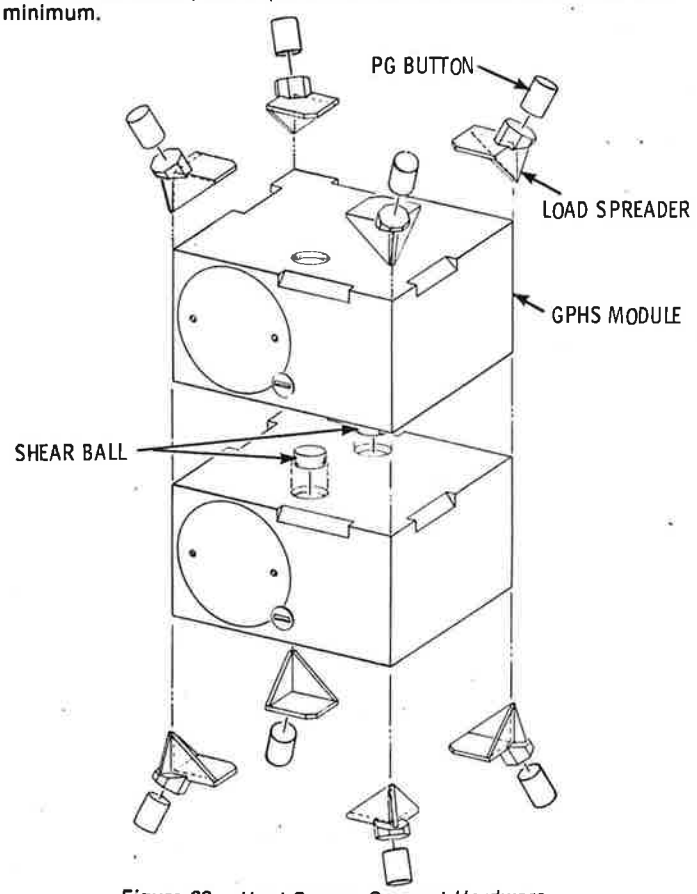

Figure 39. Heat Source Support Hardware

The preload forces are applied by Belleville springs, as illustrated in Figure 40. Note that only the upper corners of the heat source are spring-loaded. The bottom ones are rigidly connected to the generator housing.

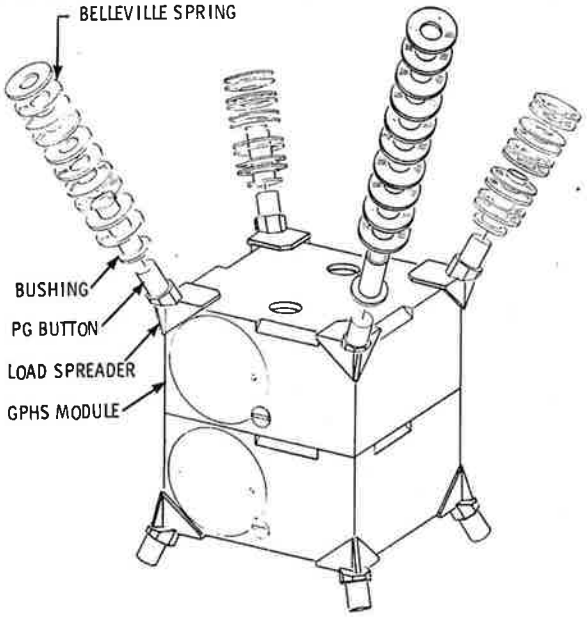

Figure 40. Heat Source Preload Springs

Belleville springs are very well-suited to this application because of their compactness and ability to deliver relatively high forces. Not too much travel is required in the present application, just enough to compensate for differential thermal growth of the heat source stack and generator housing. As shown, a total of 10 Belleville springs is required at each of the upper corners, arranged in five pairs of two. Each pair contains two springs in parallel, to double the available force. The five pairs are stacked in series, to quintuple the available travel.

Figure 41 depicts the generator end caps and the relation of the preload hardware to the top cap. As can be seen, the load-bearing points on the end cap are located near the housing flange. This is desirable because it results in primarily-tensile loads, with relatively low bending moments on the end caps. As a result, a very light end cap design is possible: basically a 0.090"-thick plate with two 0.660" by 0.090" stiffening ribs. The structural adequacy of the end cap design shown, for a 3500 lb axial preload and a 1-atmosphere pressure differential, has been confirmed by NASTRAN analysis.

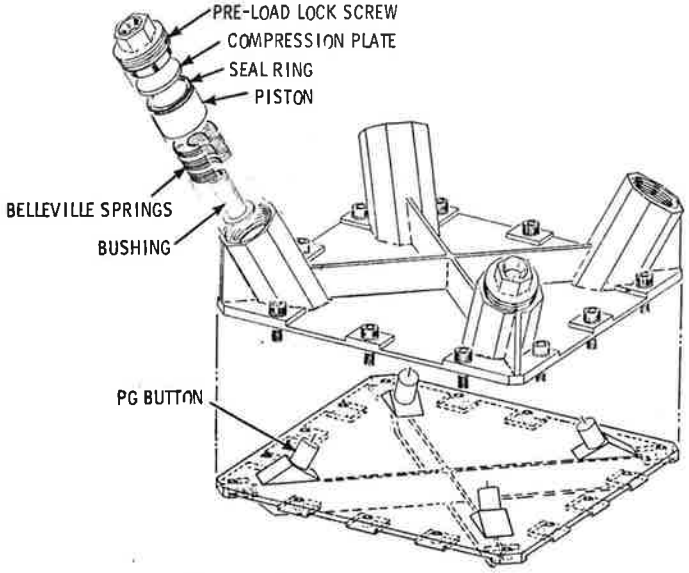

Figure 41. End Covers and Pre-Load Hardware

The detailed preload hardware is depicted in exploded view at one corner of the top cap in Figure 41 and in assembled form in the closeup section shown in Figure 42. The pyrolytic graphite button at the top of the heat source stack contacts a bushing, which is loaded by the five pairs of Belleville springs, as shown. These springs bear against a piston, which is locked in position by the preload lock screw.

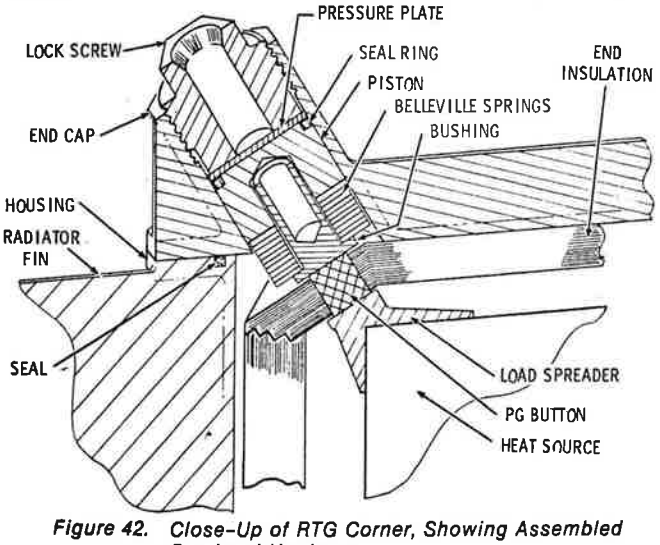

Figure 42. Close-Up of RTG Corner, Showing Assembled Pre-Load Hardware

The arrangement is designed to permit final adjustment of the preload forces after the generator is assembled and its various parts have reached their equilibrium temperature. The desired preload at each corner is applied via a pneumatic actuator or a load cell. The load is applied to the compression plate by passing a rod through the

central hole in the preload lock screw. After the load is applied and the springs have been compressed, the lock screw is tightened and the load device removed.

The ability to adjust the preload at each corner *in situ* (i.e., in the fully assembled and thermally equilibrated generator) is very important. It makes it possible to compensate for the dimensional deviation of the actual hardware from its nominal dimensions. This should allow relaxation of the tolerance specifications for various components.

GENERATOR ASSEMBLY

Figure 43 presents a cutaway view of the upper end of the assembled generator. It illustrates the geometric relationship of the heat source stack and its end supports, the thermoelectric converter modules, the multifoil thermal insulation lining the side and end walls, the generator housing with the attached radiator fins and bolted end caps, and the external electrical circuit.

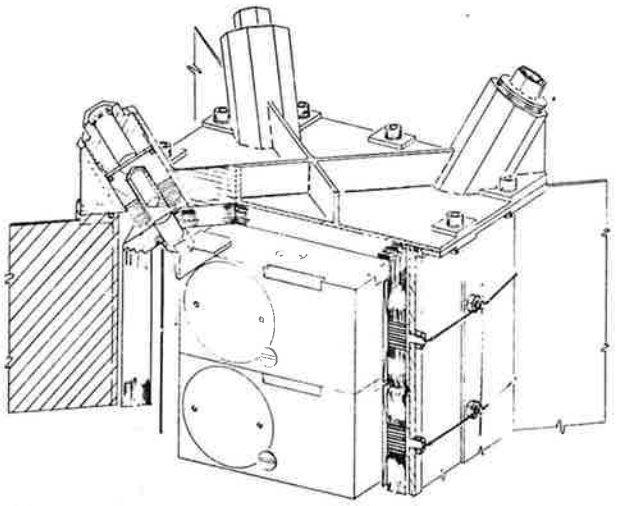

Figure 43. Cut-Away View of MITG End Section

The figure illustrates how compact and densely packed the MITG design is. The dimensions of the housing have been reduced to a near-minimum. This accounts for the low weight and high specific power of the generator.

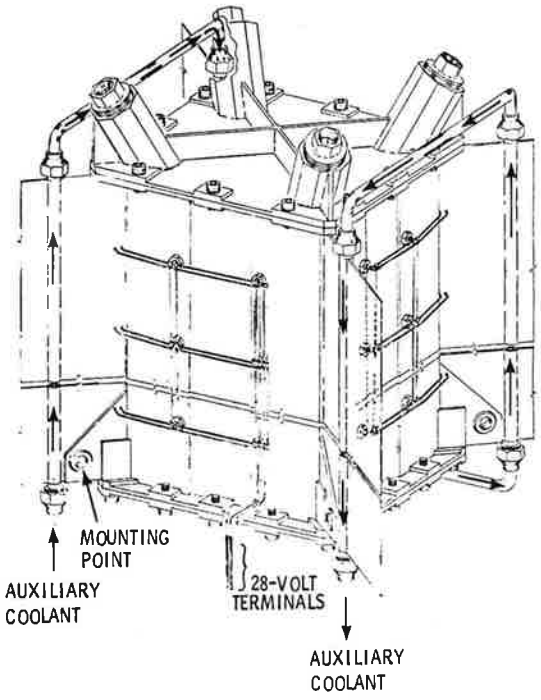

Figure 44. External View of Assembled MITG with Field-Cancelling and Redundant Circuit

A view of the fully-assembled generator is shown in Figure 44. The figure depicts the auxiliary coolant loop, and shows the mounting bushing at the base of each fin. These bushings are used for structural attachment of the cantilevered generator to the spacecraft. The electrical circuit illustrated in the figure combines the magnetic field-cancelling loops, as well as the redundant-circuit elements added for enhanced reliability against micrometeorite impact. It shows the double busbars and the 28-volt generator terminals.

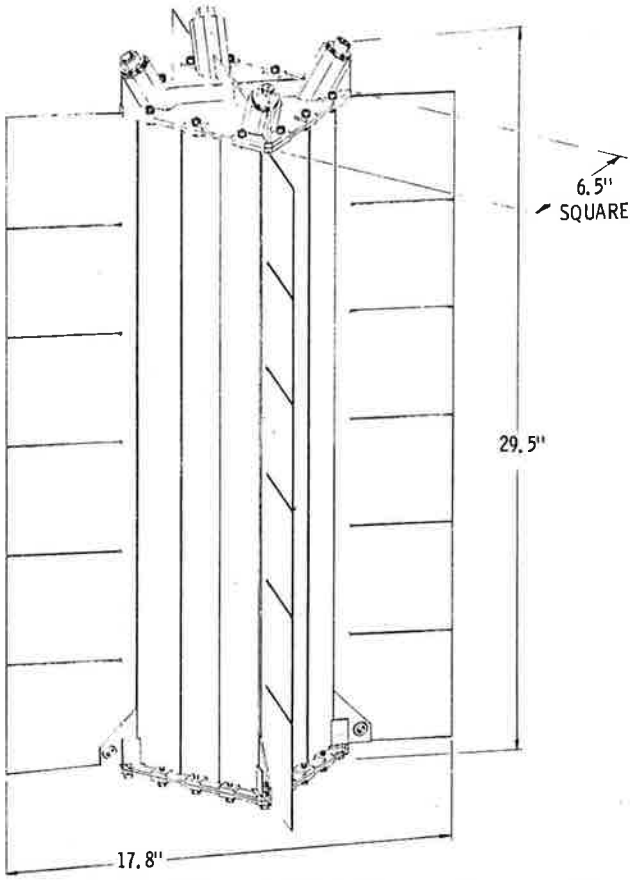

Figure 45. Typical MITG Dimensions (12 Slices, 282 Watts)

Finally, Figure 45 gives the overall dimensions of a typical 12-slice MITG (shown without electrical circuit or auxiliary coolant loop). Note that the radiator fins are slotted at 4" intervals, to reduce thermal stresses caused by temperature gradients.

WEIGHT COMPARISON

A weight summary of all the components of the generator, including some which have not been discussed in this paper, is shown in Table 2. The table presents a detailed weight breakdown for the GPHS/RTG* as well as one for a 12-slice MITG with a similar power output. Combining these breakdowns minimizes the chances of overlooking some minor or peripheral components, and facilitates comparison of the two designs. The weights of the GPHS/RTG are shown at the left of the table, the weights of the corresponding MITG components are shown at right, and the middle column shows a breakdown of the MITG weight savings.

As can be seen, there are substantial weight reductions in all four areas: the housing assembly, the converter, the heat source support system, and the heat source modules. The weight saving of the housing assembly is due to the greater compactness of the MITG design and to the better view of space from four fins instead of eight fins. In the converter, there are major weight savings due to the much smaller number of thermoelectric modules, and to the shorter leg length and simpler mounting arrangement of the thermoelectric multicouples.

There are very large weight savings in the foil insulation package, because of the elimination of quartz cloth spacers, and because the areas to be insulated are much smaller due to the compactness of the MITG. Additional weight savings result from the elimination of the insulation support frame, which is not required in the MITG design.

Table 2. Weights (Lb)

GPHS RTG (SiGe, 290 w)*			Δ	MITG (SiGe/GaP, 282 w)		
Item	No.	Wt.		Wt.	No.	Item
Housing:			10.66			
Outer Shell	1	14.25	8.25	6.00	1	
Fins	8	4.32	2.02	2.30	4	
Emissive Coating	X	0.33	0.08	0.25	X	
Auxiliary Cooling Tube Manifold	1	0.57	0.27	0.30	1	
Nuts	8	0.11	0.04	0.07	4	
Converter:			25.82			
T/E Unicouples	576	11.98	8.18	3.80	96	T/E Modules
T/E Sealing Screws	576	1.54	1.54	-	-	
T/E C-Seals	576	0.13	0.10	0.03	96	
Rivets and Washers	608	0.59	0.59	-	-	
T/E Spacers (Al_2O_3)	576	0.64	0.64	-	-	
Nut Plates	288	0.80	0.45	0.35	96	Nuts
Foil Insulation - T/P	1	13.00	10.90	2.10	1	
Foil Insulation - Ends	2	1.33	1.13	0.20	2	
Insulation Support Frame	1	1.65	1.65	-	-	
Power Connector	1	0.35		0.35	1	
Gas Management Assembly	1	0.29		0.29	1	
Electrical Straps	X	1.08	0.68	0.40	X	
PRD	1	0.90		0.90	1	
C-Seal - Domes	2	0.08	0.02	0.06	2	
Other Insulation	X	0.20	0.10	0.10	X	
Pressure Dome	2	1.25	-0.22	1.47	2	End Caps
Screws - Pressure Dome	44	0.23	0.06	0.17	32	
RTG Assembly	1	1.00		1.00	X	Pads & Bushings
Heat Source Support System:			8.41			
				0.35	8	Load Spreaders
Inboard Support	X	4.77		0.04	8	PG Buttons
				0.09	8	Bushings
Mid-Span Support	X	3.10		0.14	16	Belleville Springs
				0.32	8	Pistons
Outboard Support	X	1.85		0.06	40	Compression Plates
				0.31	8	Preload Screws
Heat Source Modules, 4464 w(t)	18	57.44	19.02	38.42	12	3000 w(t)
TOTAL		123.78	63.91	59.87		

*These weights were presented by GE at the Final Design Review of the GPHS/RTG in October 1980. They may change somewhat in the course of further development.

The MITG end caps are slightly heavier than the GPHS pressure domes, because the latter only serve to seal the housing but not to support the heat source. The GPHS/RTG employs separate titanium spiders for heat source support, and their weight is accounted for as part of the heat source support system. No such spiders are required in the MITG, since the end caps fulfill that function. This and the greater compactness of the generator account for the much lower weight of the MITG heat source support system.

The heat source weight saving is simply due to the higher thermoelectric efficiency obtained by adding gallium phosphide to silicon germanium. This allows roughly the same electrical output to be achieved with 12 instead of 18 heat source modules.

Overall, the MITG design shown weighs only about half as much as the GPHS/RTG.

EFFECT OF COLD-JUNCTION TEMPERATURE

In the discussion thus far, we have assumed a cold-junction temperature of 300°C, because that was the temperature used in the MHW and GPHS RTGs. Figure 46 illustrates how varying the cold-junction temperature affects various system parameters. The results shown are for an MITG with twelve heat source modules, eight thermoelectric modules per slice, eighteen couples per thermoelectric module, and a 1000°C hot-junction temperature. The range of cold-junction temperatures investigated is shown by tick marks at the bottom of the curve; the resultant beginning-of-life power output is shown at the bottom of the figure; and the corresponding system efficiency is shown at the top. For any given cold-junction temperature, there is an optimum fin length and fin root thickness to achieve that temperature. These are shown by tick marks at the top of the curve. The resultant generator weight is shown by the left scale, and the corresponding specific power is shown by the diagonal dotted lines.

As can be seen, the maximum specific power is achieved at a cold-junction temperature of 310°C, which is quite close to the 300°C previously assumed. It is interesting to note that the cold-junction optimum is fairly broad. Even if the radiator fins were omitted completely, the cold junction would only rise to 350°C, and the specific power would only drop from 4.72 to 4.58 w/lb. But, of course, power output and system efficiency would drop significantly if the fins were omitted. In the other direction, lowering the cold-junction temperature by increasing the fin dimensions is not too effective, because the increasing fin weight makes the specific power drop off sharply.

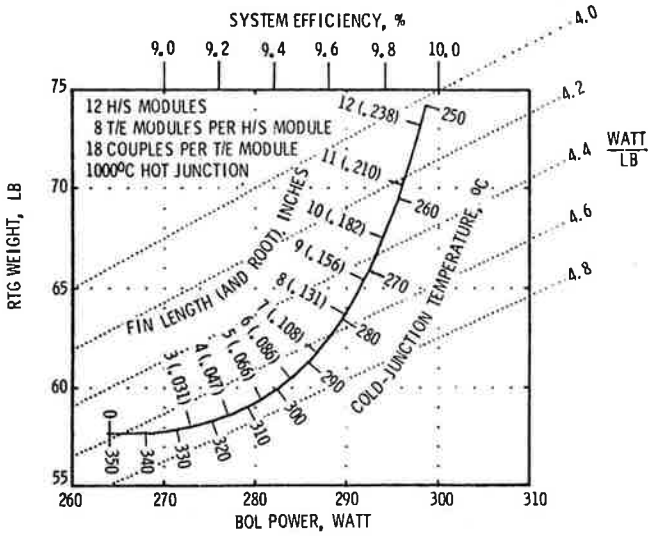

Figure 46. Effect of Cold-Junction Temperature on Optimum Fin Dimensions, RTG Weight & Power, System Efficiency, and Specific Power

The weight-vs-power curve shown in Figure 46 is for a 12-slice MITG. This curve is compared with similar curves for 11- and 13-slice MITGs in Figure 47. That figure also has the diagonal lines of constant specific power. As can be seen, for any given power level there is an optimum number of generator slices which minimizes the MITG weight.

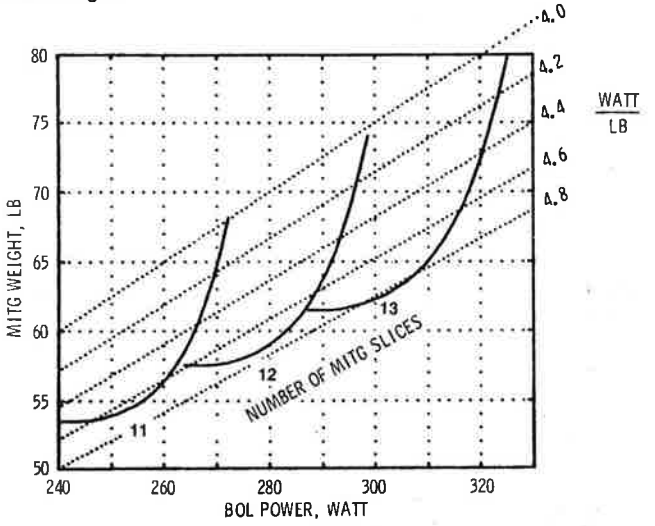

Figure 47. Weight-vs-Power Curves for Various Numbers of MITG Slices

The three curves shown are part of a much larger family of curves, and the scalloped envelop of those curves represents the maximum specific power for any given power level for the MITG design. Not surprisingly, the specific power tends to increase with power level, since the weight of the generator end sections and the associated heat losses become less significant for larger generators. The important point to note is that any desired power level can be achieved. Even though the heat source comes in discrete modules of 250 W, the generator's power output is infinitely variable by adjusting the radiator fin dimensions.

ILLUSTRATIVE DESIGN SUMMARY

Table 3 presents a design summary for the 12-slice MITG with a 300°C cold-junction temperature. It lists the number of components, principal dimensions, critical temperatures, and temperature drops. Note the large temperature drop between the fuel capsule and the heat source surface, and that between the hot-shoe corner and the hot-shoe root. The cold-end temperature drops are relatively modest in this design, but the temperature drop in the optimized radiator fins

is significant. As can be seen, the total temperature drop from the fuel capsule is about 1000°C to the generator housing, and 1100°C to the radiator fin tip; only 700°C of this is a productive temperature drop, in the thermoelectric legs.

Table 3. Design Summary (BOL)

Heat Source:		
Number of GPHS Modules	12	
Thermal Power per Module (w)	250	
BOL Thermal Power (w)	3000	
Thermoelectric Converter:		
Number of Thermoelectric Modules	96	
Number of Couples per Module	18	
Leg Width and Thickness (in)	0.057	
Module Width and Thickness (in)	0.360	
Leg Length (in)	0.300	
Generator Dimensions (in):		
Housing Side	5.75	
Heat Source Height	25	
Generator Height	27	
Generator Span	18	
Temperatures (°C):	T	ΔT
Fuel Capsule	1269	169
Heat Source Surface	1100	4
Hot-Shoe Corner	1096	76
Hot-Shoe Root	1020	20
Hot Junction	1000	700
Cold Junction	300	15
Cold Shoe	285	15
Housing	270	25
Fin Root	245	75
Fin Tip	170	

Heat Balance (w):		
Thermal Power	3000	
End Losses	75	
Side Losses	100	
Heat to TE Modules	2825	
Heat from TE Modules	2543	
Total Heat Rejection	2718	
Electrical:		
Couples in Series	144	
Couples in Parallel	12	
Module Voltage	3.50	
Module Current (amp)	0.84	
Generator Voltage	28	
Generator Current (amp)	10.1	
Power Output (w)	282	
Efficiency (%):		
Thermal (excl. module losses)	94	
Thermoelectric Material	10.5	
Thermoelectric Module	10.0	
System	9.4	
Weight (lbs):		
Heat Source	38.4	33.5
Converter	21.5	21.5
Total	59.9	55.0
Specific Power (w/lb):	4.71	5.12

Aeroshell fillets removed, and walls reduced to twice the predicted recession

The table also presents a heat balance, showing the heat losses through the end and side insulation (including the pyrographite heat source buttons) to be quite small. This accounts for the high thermal efficiency of the generator (94%).

The next block of data describes the electrical circuit, showing a module current of only 0.8 amps and a beginning-of-life power output of 282 watt. The SiGe/GaP multicouples have a material efficiency of 10.5% and a module efficiency of 10.0%. The difference between these represents both the electrical losses due to contact resistance at the hot- and cold-junctions, and the thermal losses due to heat conduction through the SiO_2 insulation. The thermal efficiency and module efficiency yield a system efficiency of 9.4% for the design. Finally, as shown earlier in Table 2, the 12-slice MITG weights 59.9 lb, and its specific power is 4.71 w/lb.

All of the numbers presented above have assumed the use of the present GPHS heat source module without any modifications. This is to permit consistent comparisons between the MITG results and corresponding numbers for the GPHS/RTG. However, for future use it is possible to identify weight reduction steps for the GPHS module [3]. Principally, this would involve reduction of the graphite aeroshell wall from 0.185" to 0.120", and elimination of internal aeroshell fillets. There are good reasons for expecting that the heat source module would still meet its safety requirements with these changes. The reduced wall thickness would still be twice the predicted ablation during reentry, and the internal aeroshell fillets serve no obvious function (see Figure 1). Their removal would leave the aeroshell as a hollow rectangular box. Once these aeroshell changes passed safety qualification, they would result in the reduced weights shown in the small column at the lower right-hand corner of Table 3. As can be seen, the use of such a modified heat source module in the MITG would increase the specific power to more than 5 watts per lb.

RELATIVE CONTRIBUTIONS OF NEW MATERIAL & NEW DESIGN

One question of considerable interest is to what extent the specific-power improvement of the MITG is due to the new thermoelectric material, and to what extent it is the result of the new design. This question is addressed in Figure 48, which seeks to separate the two effects. The results are presented in terms of past, present, and future RTGs.

The MHW generator used in the past employed a monolithic MHW heat source and SiGe unicouples; it had a specific power of 1.79 w/lb. The GPHS/RTG presently under construction for the Galileo and Solar Polar missions employs a new modular heat source and the same SiGe unicouples; it has a specific power of 2.34 w/lb. The MITG design described in this paper uses the same heat source modules as the GPHS/RTG, is based on SiGe/GaP multicouples, and employs a substantially different generator design; it has a specific power of 4.71 w/lb.

As shown in the figure, the addition of GaP to SiGe in the present GPHS/RTG design would raise its specific power to 3.02 w/lb.; conversely, the use of the MITG design with the present SiGe material would result in a specific power of 3.42 w/lb. Thus, it is clear that the new material and the new design both make important contributions to the improved specific power of the MITG. In fact, it appears that slightly more of the improvement is attributable to the new design than to the new material.

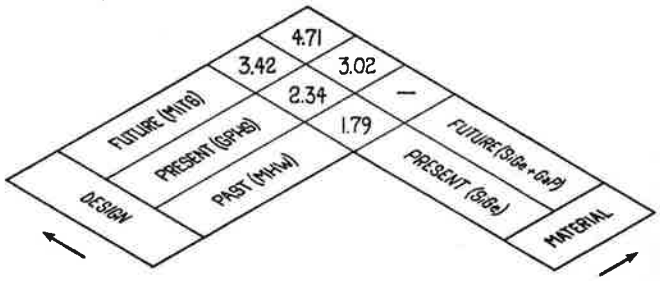

Figure 48. RTG Specific-Power Improvement (Watt/Lb)

CONCLUSION

The MITG design promises a substantially higher specific power than present-generation RTGs. This is achieved without any reduction in safety, and with probably increased reliability, because of the ability to check the performance of individual thermoelectric modules in the assembled converter, and the ability—if necessary—to replace those which are deficient. Moreover, in the long run the MITG should be more economical, because of its modularity and scalability, and because of its greater flexibility in matching the payload's voltage requirements.

It is recognized, of course, that it is risky to compare the weight of a conceptual design with that of a mature design that is actually under construction. The GPHS/RTG design has been worked out in full detail, and its weight is unlikely to change much. Although care was taken in assessing the MITG design to make certain that no parts were overlooked and to prepare realistic weight estimates for all parts, it is of course possible that its weight will grow as the result of unforeseen problems or difficulties during further development. Nevertheless, the weight advantage of the MITG is so great that there is a strong incentive for exploring this approach. DOE is therefore planning a series of tests, each consisting of a complete (electrically heated) MITG slice, to assess the feasibility and performance of that design.

Acknowledgement

The author takes pleasure in acknowledging the valuable contributions of V. Raag of Syncal, F. Huffman and staff of Thermoelectron, and T. Kline, H. Sookiazian, M. Mukunda, and E. Vogel of Fairchild.

References

[1] G.L. Bennett; B.J. Rock, "Nuclear Power Sources for Space Application", 45th Military Operations Research Symposium, US Naval Academy, June 1980.

[2a.] A.A. Pitrolo; R.B. Morrow; A.J. Arker, "Multi-Hundred Watt Radioisotope Thermoelectric Generator (MHW-RTG)", 1971 IECEC (Intersociety Energy Conversion Engineering Conference), Paper No. 719069, August 1971, Pg. 492.

[2b.] C.E. Kelly, "The MHW Converter (RTG)", 1975 IECEC, Paper No. 759132, August 1975, Pg. 880.

[3] L. Garvey; G. Stapfer, "Performance Testing of Thermoelectric Generators Including Voyager and LES 8/9 Flight Results", 1979 IECEC, Volume II, Paper No. 799312, August 1979, Pg. 1470.

[4] A. Schock, "Design Evolution and Verification of the 'Genera-Purpose Heat Source", 1980 IECEC, Volume II, Paper No. 809203, August 1980, Pg. 1032.

[5] A. Schock; H. Sooiazian, "Design Optimization of RTG for Solar-Polar Mission", 1979 IECEC, Volume II, Paper No. 799307, August 1979, Pg. 1444.

[6] R.D. Cockfield; R.F. Hartman; C.E. Kelly, "RTG Power Sources for the International Solar Polar Mission", 1980 IECEC, Volume 2, Paper No. 809204, August 1980, Pg. 1043.

[7] Michael L. Paquin, "The Multi-Foil Thermal Insulation Development Program", 1969 IECEC, Paper No. 699047, September 1969, Pg. 408.

[8] G. Stapfer; V.C. Truscello, "Sublimation Behavior of Silicon Nitride (Si_3N_4) Coated Silicon Germanium (SiGe) Unicouples", 1975 IECEC, Paper No. 759110, August 1975, Pg. 730.

[9] F.N. Huffman; S. Matsuda; G. Miskolczy; C. Wang, "Meltdown Characteristics of Multi-Foil Thermal Insulation", 1979 IECEC, Volume II, Paper No. 799298, August 1979, Pg. 1390.

[10] A. Schock; A. Shostak, "Use of Modular Heat Source Stack In RTGs", 1979 IECEC, Volume II, Paper No. 799305, August 1979, Pg. 1432.

[11] A. Shostak; A. Schock, "Dynamic Response of an RTG Cantilevered from a Shuttle-Launched Spacecraft", AIAA/ASME 21st SDM Conference, Seattle, Washington, May 1980.